Appendix to

The Chinese Silver Standard: Parity, Predictability and (In)Stability, 1912–1934

Huachen Li[†] and **James M. Nason**[‡]

April 27, 2024

[†] *e-mail*: li8@kenyon.edu, *website*: https://sites.google.com/view/huachenli, *affiliation*: Department of Economics, Ascension Hall, Kenyon College, Gambier, Ohio 43022.

[‡] *e-mail*: jmnason87@gmail.com, *website*: https://www.jamesmnason.net, *affiliations*: Centre for Applied Macroeconomic Analysis, Australian National University and Virginia Center for Economic Policy, University of Virginia.

The appendix reviews the data, identification and Bayesian estimation of the structural VARs (SVARs), several test statistics, and additional empirical results. Section A1 describes the data underlying our monthly samples of Shanghai-U.K. and Shanghai-U.S. interest rate spreads, i_t, and inflation differentials, π_t, deviations from parity of the Chinese silver standard, ρ_t, and nominal returns, Δe_t, on British pound (GBP)- and U.S. dollar (USD)-Shanghai *tael* nominal exchange rates. We discuss the necessary and sufficient conditions for global identification of the baseline SVAR in section A2. Section A3 sketches the Metropolis in Gibbs Monte Carlo Markov chain (MCMC) sampler proposed by Canova and Pérez Forero (2015a). Pseudo-code is summarized in this section that summarizes their Metropolis in Gibbs MCMC sampler. The MCMC sampler generates the posterior of a SVAR with time-varying parameters (TVPs) and errors subject to stochastic volatility (SV). Sections A4–A7 discusses computation of the TV slope coefficients of the Fama- and Engel-uncovered interest parity (UIP) regressions, the h-month ahead predictability statistic, h-month ahead forecasts, and the h-month ahead instability statistic. Further results appear in section A8.

A1. Data Construction

We draw from multiple data sources to amass the China-U.K. and China-U.S. samples on which the TVP-SV-SVARs are estimated. The data are found in Wu (1935), Shanghai Research Institute of Economics, Chinese Academy of Sciences and Research Institute of Economics, Shanghai Social Sciences Academy (1958), *Zhongguo ren min yin hang Shanghai Shi fen hang* (People's Bank of China, Shanghai Branch, 1960), Kong (1988), Ho and Lai (2016), and the NBER Macrohistory Database (MD). There are $T = 270$ observations on the 1912M04–1934M09 samples.

The U.K. and U.S. are documented having business cycle fluctuations during our sample

period, but there appears to be nothing similar for China. The NBER reports business cycle peak and trough dates at `US Business Cycle Expansions and Contractions`. These dates are available from 1857M06 to 2020M04, which accommodates our sample period. From 1912M04 to 1934M09, the U.S. experienced six recessions, according to the NBER.

We have found monthly business cycle peak and tough dates for the U.K. only in Burns and Mitchell (1946). They argued the business cycle has nines stages. Since stages V and IX cover the "three months centered on the peak" and "three months centered on the terminal trough" (Burns and Mitchell, p. 29), we equate the middle month of stage V with the peak and middle month of stage IX with the trough of the U.K. business cycle. These dates are accessible in table A1 of Burns and Mitchell (pp. 512–513) from 1854M11 to 1938M10, which shows the U.K. had six recessions from 1912M04 to 1934M09.

Table A1 of this appendix lists the months of the six peaks and six troughs of the U.K. and U.S. business cycles that occurred during our sample. These peak and trough dates define the vertical bars highlighting U.K. and U.S. recessions that are displayed in figures 1 to 6 of the paper and figures A1 to A4 of this appendix.

A1.1 Nominal short-term interest rates

Interest rate spreads are differences in nominal short-term interest rates between Shanghai, $i_{S,t}$, and London, $i_{UK,t}$, or New York City, $i_{US,t}$. These are market clearing returns in these locations and are not seasonally adjusted.

We obtain the Shanghai interbank offer rate (SHIBOR), $i_{S,t}$, from *Zhongguo ren min yin hang Shanghai Shi fen hang* (People's Bank of China, Shanghai Branch, 1960). The original sources are the *Shen Bao* (Shanghai Daily) for 1905M01 to 1917M05, *Yin Hang Zhou Bao* (Banking News) for 1917M06 to 1922M12, and *Jing Ji Tong Ji* (Economic Statistics) for the rest of the

sample. The SHIBOR is the average during a month of daily quotes from the *Shanghai Qian Ye Gong Hui* (Shanghai Banking Association). Its members met every business day at 9:00am and again in the afternoon to set the SHIBOR, but only the morning quotes are available. Pan and Long (2015) argue the SHIBOR was a market clearing interest rate because daily auctions were held by the *Shanghai Qian Ye Gong Hui* at which its members could lend or borrow funds.

The nominal short-term rate for the U.K., $i_{UK,t}$, is found in the NBER-MD. It is the 1-month return on 3-month banker's bills in the NBER-MD. This return was the open market rate of discount for London. It is labeled `M13016GB00LONM156NNBR` in FRED®.

We compile a U.S. nominal short-term interest rate, $i_{US,t}$, from three series available in the NBER-MD. The FRED® database label the series `M13001USM156NNBR`, `M13030US35620M156NNBR`, and `M1329BUSM193NNBR`. The first is U.S. call money rates (mixed collateral) from 1912M04 to 1918M12. The second short-term rate is a weighted average of open market rates in New York City (NYC). Its subsample run from 1919M01 to 1931M11. We use yields on 3- to 6-month U.S. Treasury notes and certificates and on 3-month Treasury bills from 1931M12 to 1934M09. The first splice at 1918M12–1919M01 is motivated by changes in U.S. money markets that made open market rates in New York City a better match to returns on short-term deposits in the U.S. The same plus yields on short-term Treasuries exhibit greater variation compared with returns on comparable private short-term debt motivate our second splice at 1931M11–1931M12.

Figure A1 presents plots of $i_{S,t}$, $i_{UK,t}$, and $i_{US,t}$ in percentages from 1912M04 to 1934M09. The (green) dashed, (red) dot-dash, and (blue) dotted lines denote $i_{S,t}$, $i_{UK,t}$, and $i_{US,t}$, respectively. The vertical gray shadings of the figure are NBER recession dates. The plots display greater volatility in $i_{S,t}$ than in $i_{UK,t}$ and $i_{US,t}$ by several orders of magnitude. The volatility of $i_{S,t}$ occurs during the entire sample, but is especially striking from mid 1918 to mid 1924.

These are the largest spikes in $i_{S,t}$, which are greater than 23% in 1921M11 and 1923M12. During the Great Depression, $i_{S,t}$ runs from 11 to 14% between 1931M11 and 1932M01. The next spike in $i_{S,t}$ is more than 13%, which occurred in 1934M03. The upshot is $i_{S,t}$ often ranges from less than 100 basis points to offering returns in excess of 20% during the sample.

Returns in London and NYC never exceeded 8%. Comparing $i_{UK,t}$ with $i_{US,t}$ shows the latter is more volatile than the former before 1931. After the U.K. leaves the gold standard in 1931M09, $i_{US,t}$ was less volatile and lower than $i_{UK,t}$.

The top left panel of figure 1 displays $i_{S,t} - i_{UK,t}$ and $i_{S,t} - i_{US,t}$. The plots exhibit nearly identical sawtooth paths, but $i_{S,t} - i_{UK,t}$ ($i_{S,t} - i_{US,t}$) was often negative (positive) early in the First World War from 1915M04 to 1916M03. Both spreads are smallest in 1921M02 that is in the last third of the U.K. and U.S. recessions of 1920–1921. The largest peaks in the spreads occurred in the last two months of 1923, which was about the halfway through the NBER dated 1923M05–1924M07 recession.

A1.2 Price levels and inflation

Shanghai, U.K., and U.S. price levels are measured as wholesale price indexes (WPIs). The WPIs were constructed using different bundles of commodities and intermediate goods and on different base years, but as seasonally unadjusted.

The NBER-MD is our source for U.K. WPI. We access these data from FRED® at the Federal Reserve Bank of St. Louis, which labels the U.K. WPI `M04053GBM312NNBR`. It has a base year of 1867–1877, which is changed to 1921, for the 1912M04–1934M09 sample.

The U.S. WPI is built on the NBER-MD series `M0448BUSM336NNBR` and `M0448CUSM350NNBR` found in FRED®. The former (latter) WPI ends (begins) in 1914M12 (1913M01) with a base year of 1926 (1957–1959). These WPIs are moved to the 1921 base year and spliced together in 1914

to create a WPI for the U.S. from 1912M04 to 1934M09.

We find WPIs for Shanghai in Shanghai Research Institute of Economics, Chinese Academy of Sciences and Research Institute of Economics, Shanghai Social Sciences Academy (1958) and Kong (1988). The former provides a monthly WPI with a base year of 1926 for Shanghai from 1922M01 to 1935M10. Kong (1988) reports an annual Chinese WPI from 1905 to 1921 with a base year of 1913. We create a WPI from 1905M01 to 1934M09 by moving these WPIs to a 1921 base year. Next, we interpolate the annual WPI to the monthly frequency using the methods of Chow and Lin (1971) and the U.K. and U.S. WPIs. Our monthly WPI for Shanghai is constructed by tying together the interpolated WPI and post-1921 WPI at 1921M12–1922M01.

The ARIMA X-13 estimator is applied to the seasonally unadjusted WPIs for Shanghai, the U.K., and U.S. The results are seasonally adjusted series from 1905M01 to 1934M09. The seasonally adjusted Shanghai, U.K., and U.S. WPIs are denoted $P_{S,t}$, $P_{UK,t}$, and $P_{US,t}$ and $p_{S,t} = \ln P_{S,t}$, $p_{UK,t} = \ln P_{UK,t}$, and $p_{US,t} = \ln P_{US,t}$.

We display $100p_{j,t}$ in the top left panel of figure A2 for $j = S$, UK, and US as (green) solid, (red) dot-dashed, and (blue) dashed lines from 1912M04 to 1934M09, respectively. The Shanghai WPI, although rising during the sample, is less than $p_{UK,t}$ and $p_{US,t}$ from 1916M10 to 1921M05, lay between $p_{UK,t}$ and $p_{US,t}$ from 1922M06 to 1926M12, and was greater than $p_{UK,t}$ and $p_{US,t}$ from 1929M09 to 1934M09. The reasons are rapid increases in $p_{UK,t}$ and $p_{US,t}$ during the First World War, 1919, and 1920 and a steady decline in $p_{UK,t}$ from 1925M10, which is several months after the U.K. reentered the gold standard, to the end of the sample. As a result, the U.K. returned to its pre-First World War price level by the spring of 1931. The only time $p_{US,t}$ saw a persistent decline is during the Great Depression, which the NBER dates to 1929M08–1933M03. Also, note $p_{S,t}$ increases from 1929M07 to 1931M08, falls to 1934M04,

that is followed by it rising the last five months of the sample.

The top right panel of figure A2 presents year over year inflation, $\Delta^{12}\pi_{j,t} = p_{j,t} - p_{j,t-12}$, from 1912M04 to 1934M09. These inflation rates match the same (color and) markings as for log WPIs in the top left panel of the figure. Year over year inflation in the U.K. and the U.S. display peaks of about 30% and 40% in 1917M07 and 36% and 22% in 1920M05, which were followed by deflation of -55% or more in the summer and fall of 1921, and deflation of about -20% during the Great Depression. Also, there is inverse comovement in $\Delta^{12}\pi_{S,t}$ and $\Delta^{12}\pi_{UK,t}$ or $\Delta^{12}\pi_{US,t}$ that is especially evident early and late in the samples. Shanghai WPI inflation peaked in 1920M05 at 23% while its trough was -16% in 1932M12. Hence, $\Delta^{12}\pi_{S,t}$ was not as volatile as $\Delta^{12}\pi_{UK,t}$ and $\Delta^{12}\pi_{US,t}$. Another difference is the U.K. and U.S. witnessed year over year deflation in the first half of the Great Depression while $\Delta^{12}\pi_{S,t}$ was positive from 1929M08 to 1932M01 turning to deflation for the rest of the sample.

Shanghai, U.K., and U.S. month over month WPI growth rates are in the bottom panel of figure A2 from 1912M04 to 1934M09. Month over month inflation is $\Delta\pi_{j,t} = p_{j,t} - p_{j,t-1}$. These plots are qualitatively similar to the plots of $\Delta^{12}\pi_{\ell,t}$ in panel (b) of the figure, but monthly inflation rates are choppier throughout the sample. Also observe that $\Delta\pi_{S,t}$ exhibits greater volatility compared with $\Delta\pi_{UK,t}$ and $\Delta\pi_{US,t}$ during the Great Depression.

Plots of π_t appear in the top right panel of figure 1. The smallest $\pi_{S,t} - \pi_{UK,t}$ was in 1916M12, which is the month after the end of the Battle of the Somme. The U.S. entered the First World War in 1917M04 and a month later saw the smallest $\pi_{S,t} - \pi_{US,t}$. The second smallest $\pi_{S,t} - \pi_{UK,t}$ $\left(\pi_{S,t} - \pi_{US,t}\right)$ was five months (a month) after the U.K. (U.S.) left the gold standard in 1932M02 (1933M05). Peaks in $\pi_{S,t} - \pi_{UK,t}$ and $\pi_{S,t} - \pi_{US,t}$ are in 1921M02 that is toward the end of the U.K. and U.S. recessions of the early 1920s. Both differentials had

secondary peaks during the Great Depression in 1930M06.

A1.3 Deviations from parity

We draw on Wu (1935) and Ho and Lai (2016) for deviations from parity of the Chinese silver standard. Wu equates deviations from parity, ρ_t, as the log of the nominal *GBP-tael* (*USD-tael*) exchange rate, $e_{GBP/S,t}$ $\left(e_{USD/S,t}\right)$, net of the log of the world price of silver, SP_t. The lower left panel of figure 1 plots $\rho_{j,t} = 100\left(e_{j/S,t} - SP_t\right)$, $j = GBP, USD$, which is the premium on investing in a deposit of the home country or Shanghai, China. Stationarity of ρ_t rests on $e_{j/S,t}$ and $SP_t \sim I(1)$ and that these variables share a common trend. Hence, ρ_t is the outcome of the cointegrating relationship between the *GBP*- or *USD*-Shanghai *tael* exchange rate and the world price of silver. This relationship captures the dynamic equilibrium process restoring the Chinese silver standard to parity.

There are three facts worth mentioning about ρ_t. First, the world silver market was in London or New York City during the sample. London was the home of this market from the start of the sample in 1912M04 to 1914M12 and during 1934M09, which is the last month of the sample. The move in late 1914 occurred because the silver market closed in London shortly after the First World War began. As a result, the world silver market moved to New York City. It shifted back to London after the U.S. Treasury nationalized the U.S. silver market in early August 1934; see Silber (2019, p. 64).

Next, as Jacks, Yan, and Zhao (2017) note, the concept of deviations from parity of the Chinese silver standard differs from parity under a gold standard. Parity deviations were observable and time-varying under the Chinese silver standard for two reasons. First, its parity depended on the world price of silver. The gold standard rested on posting credible domestic and foreign mint prices to define parity. In contrast, parity under the Chinese silver standard.

Second, China, the U.K., and U.S. were on different monetary standards between 1912 and 1935 because the latter two countries were on and off the gold standard during these years.

Third, Wu (1935) reports data only to 1933M12. We rely on Ho and Lai (2016) for SP_t from 1934M01 to 1934M09. However, we adjust their global market price of silver for these nine months by 0.368 pounds and 0.755 dollars per silver yuan to be consistent with the Silver Yuan Standard Plan of 1933; see Wu (1935) and Leavens (1939), among others. The plan, which was promulgated by the Nanjing Government, supplanted the several versions of *tael* used across China with the *yuan* in the form of silver coins in 1933M04. Bratter (1933) discusses that these silver coins were issued at a mint parity of 0.715 Shanghai *tael* per *yuan*, which reflects a devaluation of the Chinese currency.

The bottom left panel of figure 1 plots ρ_t. These plots depict bursts of volatility in ρ_t during the First World War, four of the six U.K. and U.S. recessions from 1918 to 1928, and the last 54 months of the samples. Peaks in ρ_t map into the largest overvaluations of $e_{GBP/S,t}$ and $e_{USD/S,t}$ in 1920M05 and 1920M12 (the first year of U.K. and U.S. recessions of 1920–1921). The largest undervaluations, or smallest ρ_t for $e_{GBP/S,t}$ and $e_{USD/S,t}$, were in 1927M08 (early in the U.K. recession of 1927M03–1928M09) and two months after the U.S. left the gold standard in 1933M06. The plots also show the Chinese silver standard took six months or less to return to parity because of mean reversion in ρ_t except at the end of the sample.

A1.4 Nominal exchange rates

Our source for $e_{GBP/S,t}$ and $e_{USD/S,t}$ is Kong (1988). She calculates $e_{GBP/S,t}$ and $e_{USD/S,t}$ as the average of three trading days, which are at the start, middle, and end of the month, from 1905M01 to 1935M10. We alter observations from 1933M04 to 1934M09 to be consistent with the Silver Yuan Standard Plan of 1933. Similar to the adjustments made to $\rho_{UK,t}$ and $\rho_{US,t}$, we

divide the exchange rates reported by Kong (1988) by the mint parity of 0.715.

The Shanghai *tael* was the preeminent unit of account for international trade in China because the port of Shanghai dominated international trade and finance for China for most of our sample; see Young (1931), Bratter (1933), Leavens (1939), Jacks, Yan, and Zhao (2017), Dean (2020), and Ma (2012, 2017, 2019). Young (1931) and Wu (1935), among others, point out there were other port cities and a few interior regions in China that established their own *tael* with different silver content. These *tael*, including the Shanghai *tael*, were fictitious units of account that were neither mediums of exchange nor stores of values.

Money markets in China traded the various units of account across the port cities and regions of China. These practices continued into the mid 1930s. Leavens (1939) and Dean (2020) discuss this history and have critical reviews. Jacks, Yan, and Zhao (2017), Ma and Zhao (2020), and Palma and Zhao (2021) present regression evidence that regional money markets in China were efficient in the sense that interest rate wedges were driven close to zero.

After the end of our sample, the Silver Yuan Standard Plan was superseded by a currency reform instituted by the Nanjing government in 1935M11. The reform established a fiat currency, the *fabi*, as legal tender in China. The *fabi* was pegged to the *GBP* and *USD* within bands set by the Nanjing government; see Leavens (1939, ch. 24) and Dean (2020, ch. 7).

Plots of $100e_{GBP/S,t}$ and $100e_{USD/S,t}$ appear in the top panel of figure A3 from 1912M04 to 1934M09. The panel has a (red) dot-dash line that is the former exchange rate and (blue) dashed line that is the latter. The exchange rates display small changes from the start of the sample to 1914, fell in the First World War with a trough in early 1920, followed by steady increases until 1931M03. Subsequently, the Shanghai *tael* depreciated against the *GBP* for the rest of the sample. However, depreciation only began for $\ln e_{USD/S,t}$ at the end of the Great

Depression when the U.S. left the gold standard.

The bottom panel of figure A3 displays year over year currency returns, $100\Delta^{12}e_{\ell/S,t} = 100\left(e_{\ell/S,t} - e_{\ell/S,t-12}\right)$, $\ell = GBP, USD$, from 1912M04 to 1934M09. The same (color and) markings are used for returns on the pound and dollar relative to the *tael* as for the log levels of the exchange rates in panel (a) of the figure. Mean reversion is the main feature of year over year nominal currency returns during the sample. During the First World War, nominal currency returns are negative. This continues into 1920, but the negative returns are more than three times greater for the return on $e_{GBP/S,t}$ compared with $e_{USD/S,t}$. There are positive returns from 1929M05 to 1931M10 on $e_{GBP/S,t}$ and from 1929M05 to 1932M01 for $e_{USD/S,t}$, but these returns are often negative for the rest of the sample. Plots of $\Delta e_{GBP/S,t}$ and $\Delta e_{USD/S,t}$ are found in the bottom right panel of figure 1.

The bottom right panel of figure 1 shows nominal currency returns took similar paths from 1912M04 to 1934M09. Bursts of volatility in $\Delta e_{GBP/S,t}$ and $\Delta e_{USD/S,t}$ occurred during the First World War, the U.K. and U.S. recessions of 1920–1921, the Great Depression, and in the summer of 1933. This volatility often coincided with $\Delta e_{GBP/S,t} < 0$ and $\Delta e_{USD/S,t} < 0$.

A1.5 Real exchange rates

Real exchange rates are defined as $q_{\ell/S,t} \equiv e_{\ell/S,t} - \left(p_{S,t} - p_{\ell,t}\right)$ for $\ell = GBP, USD$. Month over month and year over year real returns on $q_{GBP/S,t}$ and $q_{USD/S,t}$ are defined as discussed above. The top left, top right, and bottom panels of figure A4 plot $q_{GBP/S,t}$, $q_{USD/S,t}$, $100\Delta^{12}q_{GBP/S,t}$, $100\Delta^{12}q_{USD/S,t}$, $\Delta q_{GBP/S,t}$, and $\Delta q_{USD/S,t}$.

The volatility and upward drift of $\ln q_{GBP/S,t}$ and $\ln q_{USD/S,t}$ dominate the top left panel of figure A4. Another feature of the panel is that these real exchange rates display comovement with two exceptions. The gap widens between the real exchange rates from 1914 to the end

of the 1920–1921 recession and in late 1933 to early 1934. The opposite is observed after 1931M09, which is when the U.K. left the gold standard during the Great Depression.

An implication is year over year and month over month real currency returns, $\Delta q^{12}_{\ell/S,t}$ and $\Delta q_{\ell/S,t}$, often move together during the sample as observed in the top right and bottom panels of figure A4. The gap in the levels of the real exchange rates are mapped into increased volatility for these currency returns from 1915 to 1922 and in mid 1931. Spikes occur in $\Delta q_{GBP/S,t}$ and $\Delta q_{USD/S,t}$ at 1916M06, 1920M04 and 1920M06, and 1921M01 and 1921M04. There is another spike in $\Delta q_{USD/S,t}$ in 1931M07 that was proceeded by a trough in the previous month. These are the largest and smallest real currency returns observed during the sample. The smallest realization of $\Delta q_{GBP/S,t}$ is in 1931M10, which is a month after the UK left the gold standard. Troughs also occur in $\Delta q_{GBP/S,t}$ and $\Delta q_{USD/S,t}$ at 1915M12, 1916M04, 1917M09, 1919M12, 1920M08, 1921M04, and 1921M10.

A1.6 Unit root tests

Tables A2 and A3 report tests for unit roots in Shanghai, U.K., U.S., China-U.K., and China-U.S. variables from 1912M04 to 1934M09. The test statistics are t-ratios, which are obtained from augmented Dickey-Fuller (ADF) and Dickey-Fuller generalized least squares (DF-GLS) regressions. Below the t-ratios are p-values in parentheses.

We use the `arch` toolbox (v6.3.0) in *Python* (v3.10.12) to compute unit root tests. The `arch` toolbox has commands `arch.unitroot.ADF` and `arch.unitroot.DFGLS` to produce ADF and DF-GLS t-ratios and p-values. Hamilton (1994) is a good introduction to the ADF regression. Elliot, Rothenberg, and Stock (1996) propose to run a detrending regression on a time series, save the residuals, and run the DF regression on these residuals. They construct econometric theory to support their DF-GLS regression approach to test for a unit root in a time series.

Documentation for the `arch.unitroot.ADF` and `arch.unitroot.DFGLS` commands describe options for selecting the deterministic content and lag length of the regressions. We always include an intercept and a linear trend in the ADF and DF-GLS regressions. The lag length of the ADF regression is chosen using the `t-stat` option. The Akaike information criterion is employed to choose the lag length of the second DF-GLS regression. Asymptotic p-values are compiled by MacKinnon (1994, 1996, 2010).

The null hypothesis of the ADF and DF-GLS tests is a unit root in the time series. Hence, the larger is the t-ratio the smaller is the p-value. The inference is the null hypothesis is not rejected. Nevertheless, unit root tests often suffer from a lack of power against the alternative. This suggests the results are informative about the persistence or approximation to a unit root process in the variable.

There are unit root tests for $i_{S,t}$, $i_{UK,t}$, $i_{US,t}$, $\pi_{S,t}$, $\pi_{UK,t}$, $\pi_{US,t}$, $p_{S,t}$, $p_{UK,t}$, and $p_{US,t}$ in table A2. These tests offer evidence of a unit root in $i_{S,t}$, and $i_{US,t}$ with p-values of 0.47 and greater for the ADF and DF-FLS tests in the first and third rows of the table. The evidence is weaker for a unit root in $i_{UK,t}$ because the p-value of the ADF t-ratio is 0.57, but the DF-GLS test yields a p-value of 0.09. The middle three rows of table A2 show the ADF and DF-GLS tests reject the unit root null for $\pi_{S,t}$, $\pi_{UK,t}$, and $\pi_{US,t}$ with all p-values less than 10%. In no surprise, the ADF and DF-GLS tests fail to reject the null for $p_{S,t}$, $p_{UK,t}$, and $p_{US,t}$.

The last three rows of table A3 list ADF and DF-GLS t-ratios and p-values for $p_{S,t} - p_{j,t}$, $e_{\ell/S,t}$, and $q_{\ell/S,t}$, $j = UK, US$ and $\ell = GBP, USD$. Unit roots are not rejected for $p_{S,t} - p_{UK,t}$, $p_{S,t} - p_{US,t}$, $e_{GBP/S,t}$ $e_{USD/S,t}$, and $q_{USD/S,t}$, given the p-values are greater than or equal to 0.29. The ADF and DF-GLS tests yield p-values that are split on whether $q_{GBP/S,t}$ has a unit root. The p-value is zero for the DF-GLS test, but it is 0.48 for the ADF test. We infer from these

p-values that $q_{GBP/S,t}$ is persistent if not observationally equivalent to a unit root process.

The first four rows of table A3 indicate the unit null is often rejected for the variables in the China-U.K. and China-U.S. samples. The p-values show rejections at no more than a 3% level for $i_{S,t} - i_{US,t}$, $\pi_{S,t} - \pi_{UK,t}$, $\pi_{S,t} - \pi_{US,t}$, $\rho_{GBP/S,t}$, $\rho_{USD/S,t}$, $\Delta e_{GBP/S,t}$, and $\Delta e_{USD/S,t}$. The exception is $i_{S,t} - i_{UK,t}$. Its ADF test has a p-value of 0.16. The p-value is 0.08 for the DF-GLS test. Since the latter test is rejected between the 5 and 10% significance levels, $i_{S,t} - i_{UK,t}$ is treated as stationary. Hence, the TVP-SV-SVARs are estimates on stationary variables found in the China-U.K. and China-U.S. samples.

A2. Global Identification of SVAR-BL

This section applies the necessary and sufficient conditions developed by Rubio-Ramírez, Waggoner, and Zha (2010), which prove their theorem 1, to verify the global identification of our baseline SVAR, SVAR-BL, that is favored by the China-U.K. and China-U.S. samples. We reproduce the impact matrix of SVAR-BL, $\mathbf{A}_{\mathtt{BL}} = \begin{bmatrix} 1 & 0 & 0 & 0 \\ 0 & 1 & 0 & 0 \\ 0 & 0 & 1 & 0 \\ -a_{\Delta e,i} & -a_{\Delta e,\pi} & -a_{\Delta e,\rho} & 1 \end{bmatrix}$, found in equation (5) of the paper. This section works with a fixed coefficient SVAR, which is consistent with table 1 of the paper. Also, since exactly identified SVARs are the subject of theorem 2 of Bacchiocchi and Kitagawa (2021), it is not applicable to SVAR-BL, SVAR-M1, ..., SVAR-M9. Their theorem 2 holds (trivially) for our recursive SVAR, SVAR-RC, because its linear restrictions fall only on the impact matrix, $\mathbf{A}_{\mathtt{RC}}$. This makes theorem 7 of Rubio-Ramírez, Waggoner, and Zha (2010) the relevant criterion for asking whether SVAR-RC is global identified, which it (transparently) is.

Rubio-Ramírez, Waggoner, and Zha (RRWZ) develop necessary and sufficient conditions to check whether restrictions imposed on $\mathbf{A}_{\mathtt{m}}$ yield a globally identified SVAR, $\mathtt{m} = \mathtt{BL}, \mathtt{M1}, \ldots, \mathtt{M9}$. If and only if the conditions are met, are the responses of the elements of y_t to the elements of η_t measurable. The restrictions imposed on $\mathbf{A}_{\mathtt{m}}$ are bundled into the $n \times n$ matrix $\mathbf{R}_{\mathtt{m},j}$ by RRWZ such that $\mathbf{R}_{\mathtt{m},j}\,\mathbf{A}_{\mathtt{m}}'\,\ell_j = \mathbf{0}_{n\times 1}$, for $j = 1, \ldots, n$, where their transformation function $f(\cdot, \cdot) = \mathbf{A}_{\mathtt{m}}'$ because the identifying restrictions on SVAR-$\mathtt{m}$ are linear, the scale volatility matrix $\mathbf{\Sigma}_{\mathtt{m}}$ is diagonal, and ℓ_j is a $n \times 1$ selection vector with a one in its jth position.

The necessary condition of RRWZ is confirmed by first summing the ranks of $\mathbf{R}_{\mathtt{m},j}$, $\mathtt{k}_{\mathtt{m},j}$ for $j = 1, \ldots, n$. Next, compare the sum with the number of free parameters in SVAR-$\mathtt{m}$, $0.5n(n-1) = 6$, given $n = 4$. If $\sum_{j=1}^{n} \mathtt{k}_{\mathtt{m},j} \geq 6$, SVAR-$\mathtt{m}$ fulfills the necessary condition for identification. However, RRWZ note their necessary condition is equivalent to the order condition of Rothenberg (1971). There is at least as much valid information as the dimension of the parameter vector. Also, the RRWZ necessary condition is a weak restriction, but SVAR-$\mathtt{m}$ is over-identified when the inequality is strong.

There is more to verifying the sufficient condition of RRWZ. Their identification algorithm involves checking the rank of the $(n+j) \times n$ matrix $\mathcal{M}_{\mathtt{m},j} = \begin{bmatrix} \mathbf{R}_{\mathtt{m},j}\,\mathbf{A}_{\mathtt{m}}' \\ \hline \mathbf{I}_j \mid \mathbf{0}_{j\times(n-j)} \end{bmatrix}$, for $j = 1, \ldots, n$. The intuition for the rank condition is that a measurable response must exist for each of the n elements of $y_t = [i_t \;\; \pi_t \;\; \rho_t \;\; \Delta e_t]'$ to the j+1st structural shock in η_t, given this holds for jth shock, $j = 1, \ldots, n-1$. Hence, the RRWZ sufficient condition is akin to the relevance condition of instrumental variables estimators (*i.e.*, an instrument for an endogenous variable supplies additional information about it). Remember the $n = 4$ elements of η_t are the international financial, cross-country demand, risk premium, and trend exchange rate shocks.

A2.1 THE NECESSARY CONDITION FOR SVAR-BL

We solve the system of equations $\mathbf{R}_{\mathsf{BL},1}\,\mathbf{A}'_{\mathsf{BL}}\,\ell_1 = \mathbf{0}_{n\times 1}$ positing that the first column and last row of $\mathbf{R}_{\mathsf{BL},1}$ are full of zeros and its upper 3×3 block is the identity matrix

$$\begin{matrix} \mathbf{R}_{\mathsf{BL},1} & \times & \mathbf{A}'_{\mathsf{BL}} & \times\, \ell_1 & = \mathbf{0}_{4\times1} \end{matrix}$$

$$\begin{bmatrix} 0 & 1 & 0 & 0 \\ 0 & 0 & 1 & 0 \\ 0 & 0 & 0 & 1 \\ 0 & 0 & 0 & 0 \end{bmatrix} \begin{bmatrix} 1 & 0 & 0 & -a_{\Delta e,i} \\ 0 & 1 & 0 & -a_{\Delta e,\pi} \\ 0 & 0 & 1 & -a_{\Delta e,\rho} \\ 0 & 0 & 0 & 1 \end{bmatrix} \begin{bmatrix} 1 \\ 0 \\ 0 \\ 0 \end{bmatrix} = \begin{bmatrix} 0 \\ 0 \\ 0 \\ 0 \end{bmatrix}.$$

This calculation is also satisfied by

$$\mathbf{R}_{\mathsf{BL},2} = \begin{bmatrix} 1 & 0 & 0 & 0 \\ 0 & 0 & 0 & 0 \\ 0 & 0 & 1 & 0 \\ 0 & 0 & 0 & 1 \end{bmatrix}, \quad \mathbf{R}_{\mathsf{BL},3} = \begin{bmatrix} 0 & 0 & 0 & 0 \\ 1 & 0 & 0 & 0 \\ 0 & 1 & 0 & 0 \\ 0 & 0 & 0 & 1 \end{bmatrix}, \text{ and } \mathbf{R}_{\mathsf{BL},4} = \mathbf{0}_{4\times4}.$$

The restrictions embedded in $\mathbf{R}_{\mathsf{BL},1}$, $\mathbf{R}_{\mathsf{BL},2}$ $\mathbf{R}_{\mathsf{BL},3}$, and $\mathbf{R}_{\mathsf{BL},4}$ give these matrices ranks of $\mathsf{k}_{\mathsf{BL},1} = 3$, $\mathsf{k}_{\mathsf{BL},2} = 3$, $\mathsf{k}_{\mathsf{BL},3} = 3$, and $\mathsf{k}_{\mathsf{BL},4} = 0$. Hence, the necessary condition of RRWZ for SVAR-BL is satisfied because $\sum_{j=1}^{n} \mathsf{k}_{\mathsf{BL},j} = 9 \geq 6$.

A2.2 THE SUFFICIENT CONDITIONS FOR SVAR-BL

The sufficient conditions of RRWZ are applied to SVAR-BL using the rank of $\mathcal{M}_{\mathsf{m},j}$ for $j = 1, \ldots, 4$. Since we have $\mathbf{R}_{\mathsf{BL},1}$, $\mathbf{R}_{\mathsf{BL},2}$, $\mathbf{R}_{\mathsf{BL},3}$, and $\mathbf{R}_{\mathsf{BL},4}$, $\mathcal{M}_{\mathsf{BL},1} = \left[\begin{array}{cccc} 0 & 1 & 0 & -a_{\Delta e,\pi} \\ 0 & 0 & 1 & -a_{\Delta e,\rho} \\ 0 & 0 & 0 & 1 \\ 0 & 0 & 0 & 0 \\ \hline 1 & 0 & 0 & 0 \end{array}\right]$, $\mathcal{M}_{\mathsf{BL},2} =$

$$\left[\begin{array}{cccc} 1 & 0 & 0 & -a_{\Delta e,i} \\ 0 & 0 & 0 & 0 \\ 0 & 0 & 1 & 0 \\ 0 & 0 & 0 & 1 \\ \hline 1 & 0 & 0 & 0 \\ 0 & 1 & 0 & 0 \end{array}\right], \quad \boldsymbol{\mathcal{M}}_{\mathsf{BL},3} = \left[\begin{array}{cccc} 0 & 0 & 0 & 0 \\ 1 & 0 & 0 & -a_{\Delta e,i} \\ 0 & 1 & 0 & -a_{\Delta e,\pi} \\ 0 & 0 & 0 & 1 \\ \hline 1 & 0 & 0 & 0 \\ 0 & 1 & 0 & 0 \\ 0 & 0 & 1 & 0 \end{array}\right],$$ and $\boldsymbol{\mathcal{M}}_{\mathsf{BL},4}$ consists of $\mathbf{R}_{\mathsf{BL},4}$, which is a 4×4 matrix of zeros, stacked on top of $\mathbf{I}_4$. The ranks of $\boldsymbol{\mathcal{M}}_{\mathsf{BL},1}$, $\boldsymbol{\mathcal{M}}_{\mathsf{BL},2}$, $\boldsymbol{\mathcal{M}}_{\mathsf{BL},3}$, and $\boldsymbol{\mathcal{M}}_{\mathsf{BL},4}$ are $n = 4$, which affirm the sufficient conditions of RRWZ for SVAR-BL. Hence, theorem 1 of RRWZ is satisfied by SVAR-BL showing it is globally identified.

A3. The Metropolis in Gibbs MCMC sampler

We reproduce the TVP-SV-SVAR(k) of equation (6) of the paper

$$\mathbf{A}_t y_t \;=\; \mathbf{A}_t \mathbf{c}_t \;+\; \mathbf{A}_t \sum_{\ell=1}^{k} \mathbf{B}_{t,\ell} y_{t-\ell} \;+\; \boldsymbol{\Sigma}_t \eta_t, \;\; \eta_t \sim \mathcal{N}\left(\mathbf{0}_{n\times1}, \mathbf{I}_n\right), \tag{A3.1}$$

where $y_t = [i_t \;\; \pi_t \;\; \rho_t \;\; \Delta e_t]'$, $\mathbf{A}_t$ is a $n \times n$ matrix containing off-diagonal date t structural impact coefficients and only ones on the diagonal, y_t is $n \times 1$ multivariate times series, $\mathbf{c}_t$ is a $n\times1$ vector of reduced-form date t intercepts, $\mathbf{B}_{t,\ell}$ is a $n \times n$ matrix of lag ℓ date t reduced-form slope coefficients, $\boldsymbol{\Sigma}_t$ is a diagonal matrix of date t scale volatility coefficients, which are found in the vector $[\sigma_{1,t} \;\ldots\; \sigma_{n,t}]'$, η_t is a $n \times 1$ vector of structural Gaussian shocks, and $n = 4$. The TVPs and SVs evolve as (driftless) random walks (RWs) with mean zero Gaussian innovations

$$\mathbb{B}_{t+1} \quad = \quad \mathbb{B}_t \quad + \; \vartheta_{t+1}, \quad \vartheta_t \sim \mathcal{N}(\mathbf{0}, \boldsymbol{\Omega}_\vartheta), \tag{A3.2}$$

$$a_{t+1} = a_t + \psi_{t+1}, \quad \psi_t \sim \mathcal{N}(\mathbf{0}, \mathbf{\Omega}_\psi), \tag{A3.3}$$

$$\ln \gamma_{t+1} = \ln \gamma_t + \xi_{t+1}, \quad \xi_t \sim \mathcal{N}(\mathbf{0}, \mathbf{\Omega}_\xi), \tag{A3.4}$$

which are the multivariate random walks described between equations (6) and (7) of the paper, where $\mathbb{B}_t = \text{vec}([\mathbf{B}_{1,t} \ \ldots \ \mathbf{B}_{k,t} \ \mathbf{c}_t])$, a_t is a vector consisting of the off-diagonal elements of $\mathbf{A}_t$ that are non-zero, and

$$\mathcal{V} = \begin{bmatrix} \mathbf{I} & 0 & 0 & 0 \\ 0 & \mathbf{\Omega}_\vartheta & 0 & 0 \\ 0 & 0 & \mathbf{\Omega}_\psi & 0 \\ 0 & 0 & 0 & \mathbf{\Omega}_\xi \end{bmatrix}. \tag{A3.5}$$

gathers the covariance matrices of η_t and the innovations to the random walks (A3.2), (A3.3), and (A3.4) in a block diagonal covariance matrix of hyper-parameters, $\mathcal{V}$, that duplicates equation (7) of the paper.

A3.1 Our Priors on the TVP-SV-SVARs

Table A.4 lists our priors, which are empirical Bayes, on the TVP-SV-SVAR(k) of equations (A3.1)–(A3.5), where $k = 2$. We endow the initial conditions of $\mathbb{B}_t$ and a_t, $\mathbb{B}_0$ and a_0, with multivariate normal ($\mathcal{MN}$) prior distributions. Prior on the initial condition of γ_t, γ_0, is multivariate-log normal ($\mathcal{M}$–$\mathcal{LN}$). The prior means of these distributions, $\underline{\mathbb{B}}$, $\underline{a}$, and $\underline{\gamma}$, are OLS estimates of reduced-form VARs and maximum likelihood (ML) estimates of the 12 SVARs on the China-U.K. and China-U.S. samples from 1912M04 to 1934M09, where lags are 1912M02–1912M03. These estimates also provide the prior covariance matrices of $\mathbb{B}_0$, a_0, and γ_0, where $\underline{\mathbf{\Omega}}_\mathbb{B}$ is a quarter of the OLS covariance matrix of $\underline{\mathbb{B}}$ and $\underline{\mathbf{\Omega}}_a$ and $\underline{\mathbf{\Omega}}_\gamma$ are diagonal matrices with non-zero elements that are the absolute values of $\underline{a}$ and ML estimates of the SVAR variances.

We place inverse-Wishart ($\mathcal{IW}$) priors on the covariance matrices, $\underline{\mathbf{\Omega}}_{\vartheta}$ and $\underline{\mathbf{\Omega}}_{\psi}$, of the innovations to the random walks (A3.2) and (A3.3) of $\mathbb{B}_t$ and a_t. The $\mathcal{IW}$ priors have variances of $\underline{\mathbf{\Omega}}_{\mathbb{B}}$ and $\underline{\mathbf{\Omega}}_{a}$ scaled by $\kappa_{\mathbb{B}}$ and κ_a. These parameters are calibrated to achieve an acceptance rate of 50 to 60% for non-explosive draws from the posterior distribution of $\mathbb{B}_{1:T}$ and accept about 32% of the draws from the posterior distribution of $a_{1:T}$.

The innovations to the random walk (A3.4) of y_t have a diagonal covariance matrix, $\underline{\mathbf{\Omega}}_{\xi}$. Hence, the prior is on the diagonal elements, which are the variances $\sigma^2_{j,\xi}$, $j = 1, \ldots, n$. We give $\sigma^2_{j,\xi}$ an inverse-gamma ($\mathcal{IG}$) prior, which is parameterized to duplicate an $\mathcal{IW}$ distribution with two degrees of freedom and a (univariate) variance equal to the ML estimate of $\sigma^2_{j,y}$.

A3.2 The Metropolis in Gibbs MCMC Algorithm

Canova and Pérez (2015a) develop a Metropolis in Gibbs MCMC sampler that we apply to the TVP-SV-SVARs conditional on our monthly U.K.-China and U.S.-China samples and priors. The TVP-SV-SVAR of equations (A3.1) and (A3.3) is recast by CPF as a state space model. They start by writing the TVP-SV-SVAR of equation (A3.1) in concentrated form, $\mathbf{A}_t \hat{y}_t = \mathbf{\Gamma}_t \eta_t$, where $\hat{y}_t \equiv y_t - \boldsymbol{\mathcal{X}}'_t \hat{\mathbb{B}}_t$, $\hat{\mathbb{B}}_t$ is the current draw of $\mathbb{B}_t$, and $\boldsymbol{\mathcal{X}}'_t = \mathbf{I}_n \otimes \begin{bmatrix} y'_{t-1} & \ldots & y'_{t-p} & 1 \end{bmatrix}$. Next, CPF reparameterize the concentrated form of the TVP-SV-SVAR using the explicit form matrices of Amisano and Giannini (1997), $\mathbf{S}_{\mathbf{A}}$ and $\mathbf{s}_{\mathbf{A}}$. This gives a system of static regressions $\left(\hat{y}'_t \otimes \mathbf{I}_{n^2}\right)\left[\mathbf{S}_{\mathbf{A}}\, a_t + \mathbf{s}_{\mathbf{A}}\right] = \mathbf{\Gamma}_t \eta_t$, where $\text{vec}(\mathbf{A}_t) = \mathbf{S}_{\mathbf{A}}\, a_t + \mathbf{s}_{\mathbf{A}}$, $\mathbf{S}_{\mathbf{A}}$ is a $n^2 \times \dim(a_t)$ matrix of zeros and ones containing the short-run linear restrictions on $\mathbf{A}_t$, and $\mathbf{s}_{\mathbf{A}} = \text{vec}\left(\mathbf{I}_{n^2}\right)$. The static regressions have a compact form by defining $\tilde{y}'_t \equiv \left(\hat{y}'_t \otimes \mathbf{I}_{n^2}\right)\mathbf{s}_{\mathbf{A}}$ and $\boldsymbol{\mathcal{Z}}_t \equiv -\left(\hat{y}'_t \otimes \mathbf{I}_{n^2}\right)\mathbf{S}_{\mathbf{A}}$ to create the observation equations of a state space representation of the TVP-SV-SVAR, $\tilde{y}'_t = \boldsymbol{\mathcal{Z}}_t a_t + \mathbf{\Gamma}_t \eta_t$, that are linear functions of the states, a_t. Its multivariate random walk (A3.3) are the state equations that complete the state space model. First, CPF run the Kalman filter and smoother on this state

space model followed by drawing a_t in a Metropolis step.

Gibbs samplers are used by CPF to draw $\mathbb{B}_t$ and γ_t. For $\mathbb{B}_t$, they engage the Kalman filter and smoother by treating the reduced-form TVP-SV-VAR, $y_t = \boldsymbol{x}_t' \widehat{\mathbb{B}}_t + \varepsilon_t$, as the system of observation equations, where $\varepsilon_t = \mathbf{A}_t^{-1} \boldsymbol{\Gamma}_t \eta_t$. The state space model is closed by recognizing that its state equations are the multivariate random walk (A3.2) of $\mathbb{B}_t$. After operating the Kalman filter on this state space model, the Gibbs step draws $\mathbb{B}_t$ from the Kalman smoother.

Applying the Kalman filter and smoother to draw from the posterior of γ_t is more complicated. First, define $\widehat{\widehat{y}}_t \equiv \widehat{\mathbf{A}}_{0,t} \widehat{y}_t$, which equals $\boldsymbol{\Gamma}_t \eta_t$. Square both sides regression by regression and take logs to find $\ln\left(\widehat{\widehat{y}}_{\ell,t}^2 + c\right) \approx 2 \ln \gamma_{\ell,t} + \ln \eta_{\ell,t}^2$, where $\ell = 1, \ldots, n$, c is a small constant to bound the left side of the approximation away from $-\infty$, and $\ln \eta_{\ell,t}^2 \sim \ln \chi^2(1)$ with mean and variance $= \left(-1.2704,\ 0.5\pi^2\right)$; see Harvey, Ruiz, and Shephard (1994). We approximate the $\ln \chi^2(1)$ distribution with the 10-point mixture normal calibration of Omori, Chib, Shephard, and Nakajima (2007). The approximation relies on a discrete variable, $s_{\ell,t} = 1, \ldots, 10$, that reveals the state of the mixture normal distribution. The Gibbs sampler runs the Kalman filter and smoother on the state space model built on the approximate logged squared regressions and the multivariate random walk (A3.4) of γ_t to draw from its posterior conditional on $s_{\ell,t}$.

A4. TVP-Fama and TVP-Engel Regressions

The slope coefficients of the Fama regressions are computed on posteriors of the TVP-SV-SVARs and methods developed by Hodrick (1992). The Fama regressions for UIP are repeated here $\Delta e_{t+1} = \delta_{0,t} + \delta_{1,t}\left(i_{S,t} - i_{j,t}\right) + \zeta_{\Delta e,t+1}$ and $\Delta q_{t+1} = \varrho_{0,t} + \varrho_{1,t}\left(i_{j,t} - i_{S,t}\right) + \zeta_{\Delta q,t+1}$, where $j = UK, US$. Remember under UIP $\delta_{1,t} = \varrho_{1,t} = 1$. Hodrick (1992) notes the large sample OLS estimator of the slope coefficient of a forward regression is the ratio of the sum of the

autocovariances of the dependent variable and regressor to the variance of the latter. Applying this fact to the TV slope coefficients of the Fama regressions produces $\delta_{\Delta e,t} = \frac{s_{\Delta e}\boldsymbol{\mathcal{V}}_{1,t}\, s_i'}{s_i \boldsymbol{\mathcal{V}}_{0,t}\, s_i'}$ and $\delta_{\rho,t} = \frac{s_{\rho}\boldsymbol{\mathcal{V}}_{1,t}\, s_i'}{s_i \boldsymbol{\mathcal{V}}_{0,t}\, s_i'}$, where the unconditional covariance matrix of $\mathcal{Z}_t$ is

$$\boldsymbol{\mathcal{V}}_{0,t} \;=\; \texttt{reshape}\left(\left[I_{(nk)^2} - \left(\boldsymbol{\mathcal{B}}_t \otimes \boldsymbol{\mathcal{B}}_t\right)\right]^{-1} \texttt{vec}\left(\boldsymbol{\Omega}_{\Gamma,t}\right),\, nk,\, nk\right), \tag{A4.1}$$

which relies on $\texttt{vec}\left(\mathcal{T}_1\mathcal{T}_2\mathcal{T}_3\right) = \left(\mathcal{T}_3' \otimes \mathcal{T}_1\right)\texttt{vec}\left(\mathcal{T}_2\right)$ when vectorizing three conformable matrices, where the companion matrix

$$\boldsymbol{\mathcal{B}}_t \;\equiv\; \begin{bmatrix} \mathbf{B}_{1,t} & \mathbf{B}_{2,t} & \dots & \mathbf{B}_{k-1,t} & \mathbf{B}_{k,t} \\ \mathbf{I}_n & \mathbf{0}_{n\times n} & \dots & \mathbf{0}_{n\times n} & \mathbf{0}_{n\times n} \\ \mathbf{0}_{n\times n} & \mathbf{I}_n & \dots & \mathbf{0}_{n\times n} & \mathbf{0}_{n\times n} \\ \vdots & \vdots & \ddots & \vdots & \vdots \\ \mathbf{0}_{n\times n} & \mathbf{0}_{n\times n} & \dots & \mathbf{I}_n & \mathbf{0}_{n\times n} \end{bmatrix},$$

$\otimes$ denotes the Kronecker product, $\boldsymbol{\Omega}_{\Gamma,t} = \Gamma_t\Gamma_t'$ is a $nk \times nk$ matrix full of zeros except that its upper left $n \times n$ block contains $\mathbf{E}_t\left\{\mathbf{A}_t^{-1}\boldsymbol{\Sigma}_t\eta_t\eta_t'\boldsymbol{\Sigma}_t'\left(\mathbf{A}_t^{-1}\right)'\right\}$, treating $\mathbf{A}_t$, C_t, $\boldsymbol{\mathcal{B}}_t$, and $\boldsymbol{\Sigma}_t$ as predetermined, and the first autocovariance matrix of $\mathcal{Z}_t$ is $\boldsymbol{\mathcal{V}}_{1,t} = \boldsymbol{\mathcal{B}}_t\boldsymbol{\mathcal{V}}_{0,t}$.

Engel (2016) emphasizes that the signs of $\text{cov}(\mathbf{E}_t\rho_{t+1},\, r_t)$ and $\text{cov}\left(\mathbf{E}_t\sum_{j=0}^{\infty}\rho_{t+j+1},\, r_t\right)$ provide evidence about UIP. When the covariance equals zero, UIP holds. Otherwise, there is excess movement in the response of the real exchange rate, q_t, to the real interest rate spread, r_t.

Evidence about the sign of $\text{cov}_t\left(\mathbf{E}_t\sum_{j=0}^{\infty}\rho_{t+j+1},\, r_t\right)$ is also generated using methods developed by Hodrick (1992). He considers the problem of regressing a dependent variable that sums h-period ahead returns on a date t explanatory variable (and an intercept). The problem is, as Hodrick (1992) emphasizes, evaluating the small sample properties of tests of the slope

coefficient. The assessment rests on constructing a valid standard error of the slope coefficient, which is difficult because of the obvious serial correlation in the error term. Hodrick proposes a fix that regroups the dependent variable and regressor into a regression of the 1-period ahead return on the explanatory variable summed from date $t-h+1$ to date t.

We follow Hodrick (1992) to specify regressions with TV-slope coefficients that mimic the signs of $\text{cov}_t\left(\mathbf{E}_t\rho_{t+1},\, r_{j,t}-r_{S,t}\right)$ and $\text{cov}_t\left(\mathbf{E}_t\sum_{j=0}^{\infty}\rho_{t+j+1},\, r_{j,t}-r_{S,t}\right)$. He regroups a regression of $\sum_{j=1}^{H}\rho_{t+j}$ on a constant and $r_{j,t}-r_{S,t}$ into a regression of ρ_{t+1} on a constant and $\sum_{j=0}^{H-1}\left(r_{j,t-j}-r_{S,t-j}\right)$. For $H=1$, the sign of $\text{cov}_t\left(\mathbf{E}_t\rho_{t+1},\, r_t\right)$ is recovered from the TV-slope coefficient of the regression, $\rho_{t+1}=\phi_{0,t}+\phi_{1,t}\left(r_{j,t}-r_{S,t}\right)+\zeta_{\rho,t+1}$. We approximate the sign of $\text{cov}_t\left(\mathbf{E}_t\sum_{j=0}^{\infty}\rho_{t+j+1},\, r_t\right)$ with the TV-slope coefficient of the long-horizon regression $\rho_{t+1}=\phi_{0,t}+\phi_{H,t}\sum_{h=0}^{H-1}\left(r_{j,t-h}-r_{S,t-h}\right)+\zeta_{\rho,t+1}$ and replicate it as $H\to\infty$.

We adapt Hodrick's approach to test UIP by approximating the regression implied by $\text{cov}\left(\mathbf{E}_t\sum_{j=0}^{\infty}\rho_{t+j+1},\, r_t\right)$. The covariance is the numerator of the slope coefficient obtained by regressing the infinite forward sum of parity deviations starting at date $t+1$ on r_t. The approximating regression truncates the infinite horizon of the sum at horizon h. Hodrick's proposal maps the approximating regression into $\rho_{t+1}=\phi_{0,t}+\phi_{h,t}r_{t,h}+\lambda_{h,t+1}$, where $r_{t,h}=\sum_{j=0}^{h-1}r_{t-j}$. At horizon h, $\phi_{h,t}$ approximates the sign of $\text{cov}_t\left(\mathbf{E}_t\sum_{j=0}^{\infty}\rho_{t+j+1},\, r_t\right)$ and replicates the sign as $h\longrightarrow\infty$. The regression is estimable because ρ_t is observed in the Chinese Silver Standard sample, which differs from the floating rate period studied by Engel (2016).

Similar to the previous section, the large sample OLS estimator of $\vartheta_{h,t}$ is the ratio of explained to total variation. The ratio equates $\phi_{h,t}$ to $\dfrac{s_\rho\boldsymbol{\mathcal{V}}_{h,t}\,s_r'}{s_r\boldsymbol{\mathcal{V}}_{0,t}\,s_r'}$, where the autocovariance at lag h is $\boldsymbol{\mathcal{V}}_{h,t}=\sum_{j=1}^{h}\boldsymbol{\mathcal{B}}_t^j\boldsymbol{\mathcal{V}}_{0,t}$ and $s_r=s_i-s_\pi\boldsymbol{\mathcal{B}}_t$. The selection vector s_r reflects that the real rate spread, r_t, equals $i_t-\mathbf{E}_t\pi_{t+1}$.

A5. Calculating Forecast Predictability

An assessment of the predictable content of z_t is found in the $\mathcal{R}^2_{z,h,t}$ statistic of Cogley, Primiceri, and Sargent (2010). They measure the h-month ahead predictability of z_t at date t as one minus the ratio of its conditional variance to its unconditional variance, given the anticipated utility model (AUM) holds (*i.e.*, $\left(\boldsymbol{\mathcal{B}}_{t+j} = \boldsymbol{\mathcal{B}}_t^j\right)$. Recasting the Cogley et al predictability statistic at forecast horizon h in our notation gives

$$\mathcal{R}^2_{z,h,t} \approx 1 - \frac{s_z\left[\sum_{j=0}^{h-1} \boldsymbol{\mathcal{B}}_t^j \boldsymbol{\Omega}_{\Gamma,t}\left(\boldsymbol{\mathcal{B}}_t^j\right)'\right] s_z'}{s_z\left[\sum_{j=0}^{\infty} \boldsymbol{\mathcal{B}}_t^j \boldsymbol{\Omega}_{\Gamma,t}\left(\boldsymbol{\mathcal{B}}_t^j\right)'\right] s_z'}, \tag{A5.1}$$

where $z = i,\ \pi,\ \rho_t$, or Δe. Unpredictability of z_t translates into $\mathcal{R}^2_{z,h,t} = 0$ for all h and dates t while $\lim_{h\to\infty} \mathcal{R}^2_{z,h,t} = 0$. We also recover $\mathcal{R}^2_{x,h,t}$ for r_t by replacing s_z with s_r in equation (A5.1).

The $\mathcal{R}^2_{z,h,t}$ statistic is computed by taking the vector operator, $\mathsf{vec}(\cdot)$ through the numerator and denominator of equation (A5.1). In the denominator, the infinite sum $\sum_{j=0}^{\infty} \boldsymbol{\mathcal{B}}_t^j \boldsymbol{\Omega}_{\Gamma,t}\left(\boldsymbol{\mathcal{B}}_t^j\right)'$ $= \left[I_{n^2} - \left(\boldsymbol{\mathcal{B}}_t \otimes \boldsymbol{\mathcal{B}}_t\right)\right]^{-1} \mathsf{vec}\left(\boldsymbol{\Omega}_{\Gamma,t}\right)$. Hence $\boldsymbol{\mathcal{V}}_{0,t} = \sum_{j=0}^{\infty} \boldsymbol{\mathcal{B}}_t^j \boldsymbol{\Omega}_{\Gamma,t}\left(\boldsymbol{\mathcal{B}}_t^j\right)'$. The finite sum in the numerator, $\sum_{j=0}^{h-1} \boldsymbol{\mathcal{B}}_t^j \boldsymbol{\Omega}_{\Gamma,t}\left(\boldsymbol{\mathcal{B}}_t^j\right)'$, is the difference of the infinite sums, $\sum_{j=0}^{\infty} \boldsymbol{\mathcal{B}}_t^j \boldsymbol{\Omega}_{\Gamma,t}\left(\boldsymbol{\mathcal{B}}_t^j\right)'$ and $\sum_{j=h}^{\infty} \boldsymbol{\mathcal{B}}_t^j \boldsymbol{\Omega}_{\Gamma,t}\left(\boldsymbol{\mathcal{B}}_t^j\right)'$. Applying the change of index $j = \ell + h$ to the latter infinite sum results in

$$\sum_{j=h}^{\infty} \boldsymbol{\mathcal{B}}_t^j \boldsymbol{\Omega}_{\Gamma,t}\left(\boldsymbol{\mathcal{B}}_t^j\right)' = \sum_{\ell=0}^{\infty} \boldsymbol{\mathcal{B}}_t^{\ell+h} \boldsymbol{\Omega}_{\Gamma,t}\left(\boldsymbol{\mathcal{B}}_t^{\ell+h}\right)' = \boldsymbol{\mathcal{B}}_t^h \left[\sum_{\ell=0}^{\infty} \boldsymbol{\mathcal{B}}_t^{\ell} \boldsymbol{\Omega}_{\Gamma,t}\left(\boldsymbol{\mathcal{B}}_t^{\ell}\right)'\right]\left(\boldsymbol{\mathcal{B}}_t^h\right)'.$$

Next, pass the $\mathsf{vec}(\cdot)$ operator through the infinite sum to the right of the second equality

$$\mathsf{vec}\left(\boldsymbol{\mathcal{B}}_t^h \left[\sum_{\ell=0}^{\infty} \boldsymbol{\mathcal{B}}_t^{\ell} \boldsymbol{\Omega}_{\Gamma,t}\left(\boldsymbol{\mathcal{B}}_t^{\ell}\right)'\right]\left(\boldsymbol{\mathcal{B}}_t^h\right)'\right) = \left(\boldsymbol{\mathcal{B}}_t^h \otimes \boldsymbol{\mathcal{B}}_t^h\right) \mathsf{vec}\left(\boldsymbol{\mathcal{V}}_{0,t}\right),$$

where $\boldsymbol{\mathcal{V}}_{0,t} = \sum_{\ell=0}^{\infty} \boldsymbol{\mathcal{B}}_t^{\ell} \boldsymbol{\Omega}_{\Gamma,t}\left(\boldsymbol{\mathcal{B}}_t^{\ell}\right)'$. The column vector to the right of the equality is reshaped

to produce $\boldsymbol{\mathcal{V}}_{\mathcal{B},h,t} \equiv \texttt{reshape}\left(\left(\boldsymbol{\mathcal{B}}_t^h \otimes \boldsymbol{\mathcal{B}}_t^h\right) \texttt{vec}\left(\boldsymbol{\mathcal{V}}_{0,t}\right), nk, nk\right)$ remembering that $\boldsymbol{\mathcal{V}}_{\mathcal{B},h,t} = \boldsymbol{\mathcal{B}}_t^h \boldsymbol{\mathcal{V}}_{0,t} \left(\boldsymbol{\mathcal{B}}_t^h\right)'$. Substituting these results into the numerator and denominator in equation (A5.1) yields the approximation

$$\mathcal{R}^2_{z,h,t} \approx 1 - \frac{s_z \left[\boldsymbol{\mathcal{V}}_{0,t} - \boldsymbol{\mathcal{V}}_{\mathcal{B},h,t}\right] s_z'}{s_z \boldsymbol{\mathcal{V}}_{0,t} s_z'}. \tag{A5.2}$$

Equation (A5.2) makes clear $\mathcal{R}^2_{z,h,t} \in [0,1)$ month by month.

A6. Generating h-Month Ahead Forecasts

The TVP-SV-SVAR(k) of equation (A3.1) has a reduced form

$$\mathcal{Z}_t = C_t + \boldsymbol{\mathcal{B}}_t \mathcal{Z}_{t-1} + \Gamma_t, \tag{A6.1}$$

where $\mathcal{Z}_t \equiv \left[\mathcal{Y}_t' \; \mathcal{Y}_{t-1}' \ldots \mathcal{Y}_{t-k+1}'\right]'$, $C_t \equiv \left[\mathbf{c}_t' \; \mathbf{0}_{1\times n} \ldots \mathbf{0}_{1\times n}\right]'$, $\Gamma_t \equiv \left[\left(\mathbf{A}_t^{-1}\boldsymbol{\Sigma}_t \eta_t\right)' \; \mathbf{0}_{1\times n} \ldots \mathbf{0}_{1\times n}\right]'$. Equation (A6.1) is a VAR(1) in companion form. It yields the 1-month ahead forecast $\mathbf{E}_t z_{t+1} = s_z \left[\widetilde{C}_t + \widetilde{\boldsymbol{\mathcal{B}}}_t \hat{\mathcal{Z}}_t\right]$, where $\mathbf{E}_t\{\cdot\}$ conditions on the history of $\mathcal{Y}_t$, TVPs, and SV through date t $\left(\textit{i.e.}, \mathcal{Y}^t = \left[\mathcal{Y}_t \; \mathcal{Y}_{t-1} \ldots \mathcal{Y}_1\right]$, $\mathbf{c}^t$, $\mathbb{B}^t$, and $\gamma^t\right)$, and the hyper-parameters $\boldsymbol{\Omega}_\vartheta$ and $\boldsymbol{\Omega}_\xi$, s_z is a vector with $nk-1$ zeros and a one in any of its first n $(=4)$ positions to select z_t as i_t, π_t, ρ_t, or Δe_t, $\widetilde{C}_t$ and $\widetilde{\boldsymbol{\mathcal{B}}}_t$ denote a $nk\times 1$ vector and a $nk\times nk$ matrix that contain posterior draws from the TVP-SV-VAR(k), and $\hat{\mathcal{Z}}_t$ is the Kalman filtered prediction of $\mathcal{Z}_t$.

Calculating forecasts longer than 1-month ahead is difficult in the presence of TVPs. Motivated by the anticipated utility model (AUM) of Kreps (1998), we employ a local approximation. It generates h-month forecasts of $\mathbf{E}_t z_{t+h}$, by matching future realizations of the TVPs with the current realizations, $\widetilde{C}_t$ and $\widetilde{\boldsymbol{\mathcal{B}}}_t$; see Cogley and Sbordone (2008) and Cogley, Primiceri, and Sargent (2010). Hence, the 1-month ahead forecast is $\mathbf{E}_t z_{t+1} = s_z \left[\widetilde{C}_t + \widetilde{\boldsymbol{\mathcal{B}}}_t \hat{\mathcal{Z}}_t\right]$ while the h-month ahead forecast is $\mathbf{E}_t z_{t+h} = s_z \left[\left(\mathbf{I}_{nk} - \boldsymbol{\mathcal{B}}_t^h\right)\left(\mathbf{I}_{nk} - \boldsymbol{\mathcal{B}}_t\right)^{-1} \widetilde{C}_t + \widetilde{\boldsymbol{\mathcal{B}}}_t^h \hat{\mathcal{Z}}_t\right]$, where the expec-

tation conditions on $\mathcal{Y}^t$, $\mathbf{c}^t$, $\mathbb{B}^t$, $\mathcal{Y}^t$, $\mathbf{\Omega}_\vartheta$, and $\mathbf{\Omega}_\xi$ and $\left(\mathbf{I}_{nk} - \boldsymbol{\mathcal{B}}_t^h\right)\left(\mathbf{I}_{nk} - \boldsymbol{\mathcal{B}}_t\right)^{-1} = \sum_{j=0}^{h-1} \widetilde{\boldsymbol{\mathcal{B}}}_t^j$. These predictions aid in computing accumulated h-month ahead forecasts, $\mathbf{E}_t\left\{z_{t+h} - z_t\right\} = \mathbf{E}_t \sum_{j=1}^{h} \Delta z_{t+j}$. Building on insights in Cogley and Sargent (2015) and Nason and Smith (2023), apply the relevant elements of the multivariate random walk (A3.2) to C_t and the hypothesis of the AUM to $\boldsymbol{\mathcal{B}}_t$ while summing Δz_t over a h-month horizon using the reduced form VAR(1) of equation (A3.1) to generate $\mathbf{E}_t\left\{z_{t+1} - z_t\right\} = s_z\left[\widetilde{C}_t + \left(\widetilde{\boldsymbol{\mathcal{B}}}_t - \mathbf{I}_{nk}\right)\hat{\mathcal{Z}}_t\right]$ and for $h \geq 2$

$$\mathbf{E}_t\left\{z_{t+h} - z_t\right\} = s_z\left[\sum_{j=0}^{h-1} \widetilde{\boldsymbol{\mathcal{B}}}_t^j \widetilde{C}_t + \left(\widetilde{\boldsymbol{\mathcal{B}}}_t^h - \mathbf{I}_{nk}\right)\hat{\mathcal{Z}}_t\right], \tag{A6.2}$$

where for $j = 0$, $\widetilde{\boldsymbol{\mathcal{B}}}_t^j \equiv \mathbf{I}_{nk}$. Forecasts of the real rate spread, r_t, are generated from equation (A6.2) using $\mathbf{E}_t\left\{r_{t+h} - r_t\right\} = s_i \mathbf{E}_t\left\{\hat{\mathcal{Z}}_{t+h} - \hat{\mathcal{Z}}_t\right\} - s_\pi \mathbf{E}_t\left\{\hat{\mathcal{Z}}_{t+h+1} - \hat{\mathcal{Z}}_t\right\}$, where the right hand side of the equality reflects the forecast of the nominal rate spread net of 1-month ahead expected inflation, $i_t - \mathbf{E}_t \pi_{t+1}$.

We also produce forecasts of $\mathbf{E}_t\left\{p_{t+h} - p_t\right\}$ and $\mathbf{E}_t\left\{e_{t+h} - e_t\right\}$. The forecast of the sum of nominal currency returns from 1- to h-months ahead is

$$\mathbf{E}_t\left\{e_{t+h} - e_t\right\} = s_{\Delta e}\left[\left(h\mathbf{I}_{nk} - \sum_{j=1}^{h} \widetilde{\boldsymbol{\mathcal{B}}}_t^j\right)\left(\mathbf{I}_{nk} - \widetilde{\boldsymbol{\mathcal{B}}}_t\right)^{-1} \widetilde{C}_t + \sum_{j=1}^{h} \widetilde{\boldsymbol{\mathcal{B}}}_t^j \hat{\mathcal{Z}}_t\right], \tag{A6.3}$$

which relies on the formulas for $\mathbf{E}_t z_{t+1}$ and $\mathbf{E}_t z_{t+h}$ found above. Substitute s_π for s_z in equation (A6.3) to obtain the forecast for the sum of expected inflation from 1- to h-months ahead.

A7. Measuring Instability of the Chinese Silver Standard

Instability in $e_{GBP/S,t}$ and $e_{USD/S,t}$ is measured as $\left[\mathcal{V}_t\left(e_{t+h} - \mathbf{E}_t e_{t+h}\right) + \left(\mathbf{E}_t e_{t+h} - e_t\right)^2\right]^{1/2}$, which is in equation (8) of Cogley and Sargent (2015). The first component is the conditional variance, $\mathcal{V}_t\left(e_{t+h} - \mathbf{E}_t e_{t+h}\right)$, that is grounded in the h-month ahead forecast innovation. The

other piece is $\left(\mathbf{E}_t e_{t+h} - e_t\right)^2$. It is the mean square error (MSE) of the sum of h-month ahead forecasts of Δe_t found using equation (A6.2) at $z = \Delta e$. As a result, the building blocks of the instability measure are the TVP-SV-SVAR of equation (A3.1) in the VAR(1) companion form of equation (A6.1), the multivariate random walk (A3.2) as it pertains to C_t, and the implications of the AUM for $\boldsymbol{\mathcal{B}}_t$ and the multivariate geometric random walk (A3.4) of the SVs. Since the conditional variance $\mathbf{E}_t\left\{\left(e_{t+h} - \mathbf{E}_t e_{t+h}\right)^2\right\} \equiv \mathcal{V}_t\left(\sum_{j=1}^{h}\left[\Delta e_{t+j} - \mathbf{E}_t \Delta e_{t+j}\right]\right)$, we use the reduced form VAR(1) of equation (A6.1) to construct h-month ahead forecast errors of $\Delta e_t = s_{\Delta e}\mathcal{Z}_t$.

We construct the conditional variance $\left(E_t e_{t+h} - e_t\right)^2$ assuming the intercept and lag TVPs are known at year t. The result is

$$\left(\mathbf{E}_t e_{t+h} - e_t\right)^2 \;=\; s_{\Delta e}\left[\sum_{j=1}^{h} \boldsymbol{\mathcal{B}}_t^j \,\mathbf{E}_t\left\{\mathcal{Z}_t \mathcal{Z}_t'\right\}\left(\sum_{j=1}^{h} \boldsymbol{\mathcal{B}}_t^j\right)'\right] s_{\Delta e}'. \tag{A7.1}$$

Substitute $\boldsymbol{\mathcal{B}}_t\left(\mathbf{I}_{nk} - \boldsymbol{\mathcal{B}}_t^h\right)\left(\mathbf{I}_{nk} - \boldsymbol{\mathcal{B}}_t\right)^{-1}$ for $\sum_{j=1}^{h} \boldsymbol{\mathcal{B}}_t^j$ on the right hand side of equation (A7.1) and remember equation (A4.1) sets the unconditional variance of $\mathcal{Z}_t$, $\boldsymbol{\mathcal{V}}_{0,t} = \mathbf{E}_t\left\{\mathcal{Z}_t \mathcal{Z}_t'\right\}$, to compute the MSE of the sum of h-month ahead forecasts of Δe_t.

The 1-month ahead exchange rate forecast error $e_{t+1} - \mathbf{E}_t e_{t+1}$ equals the currency return forecast error at the same horizon, $\Delta e_{t+1} - \mathbf{E}_t \Delta e_{t+1}$. Pushing the VAR$(1)$ of equation (A6.1) ahead a period, passing the expectations operator through, and calculating the differing yields $e_{t+1} - \mathbf{E}_t e_{t+1} = s_{\Delta e}\left[C_{t+1} - C_t + \left(\mathbf{I}_{nk} - \mathbf{E}_t\right)\boldsymbol{\mathcal{B}}_{t+1}\mathcal{Z}_t + \Gamma_{t+1}\right]$, where differences across $\widetilde{C}_t$ and C_t and $\widetilde{\boldsymbol{\mathcal{B}}}_t$ and $\boldsymbol{\mathcal{B}}_t$ are ignored. Define $\vartheta_{C,t+1}$ as the $nk\times 1$ vector containing the innovations of the TV intercepts in its first n elements and zeros in the remaining $n(k-1)$ positions. Substitute it for $C_{t+1} - C_t$ to produce $e_{t+1} - \mathbf{E}_t e_{t+1} = s_{\Delta e}\left[\vartheta_{C,t+1} + \left(\mathbf{I}_{nk} - \mathbf{E}_t\right)\boldsymbol{\mathcal{B}}_{t+1}\mathcal{Z}_t + \Gamma_{t+1}\right]$.

The process becomes more complicated at $h \geq 2$. First, note the h-month ahead exchange rate forecast error $e_{t+h} - \mathbf{E}_t e_{t+h} \equiv \Delta e_{t+h} - \mathbf{E}_t \Delta e_{t+h} + e_{t+h-1} - \mathbf{E}_t e_{t+h-1}$. Lag the recursion a

month, substitute the result for $e_{t+h-1} - \mathbf{E}_t e_{t+h-1}$ and repeat $h-2$ times to find $e_{t+h} - \mathbf{E}_t e_{t+h}$ $= \sum_{j=1}^{h} \left(\Delta e_{t+j} - \mathbf{E}_t \Delta e_{t+j} \right)$. The result sets the h-month ahead exchange rate forecast error to the sum of currency return forecast errors from 1-month to h-months ahead. Hence, given the 1-month ahead currency return forecast error, we only need to compute the currency return forecast error at $h = 2$ to obtain $e_{t+2} - \mathbf{E}_t e_{t+2}$ and so on.

Repeating the process of pushing VAR(1) of equation (A6.1) ahead (this time) two periods, applying the expectations operator, and taking differences produces the 2-month ahead forecast error of the currency return

$$\Delta e_{t+2} - \mathbf{E}_t \Delta e_{t+2} = s_{\Delta e} \Big[C_{t+2} - C_t + \left(\mathbf{I}_{nk} - \mathbf{E}_t \right) \Big[\boldsymbol{\mathcal{B}}_{t+2} C_{t+1} + \boldsymbol{\mathcal{B}}_{t+2} \boldsymbol{\mathcal{B}}_{t+1} \mathcal{Z}_t \Big] + \Gamma_{t+2} + \boldsymbol{\mathcal{B}}_{t+2} \Gamma_{t+1} \Big].$$

Adding the previous equation to $e_{t+1} - \mathbf{E}_t e_{t+1} = s_{\Delta e} \Big[\vartheta_{C,t+1} + \left(\mathbf{I}_{nk} - \mathbf{E}_t \right) \boldsymbol{\mathcal{B}}_{t+1} \mathcal{Z}_t + \Gamma_{t+1} \Big]$ gives

$$\begin{aligned} e_{t+2} - \mathbf{E}_t e_{t+2} &= s_{\Delta e} \Bigg[\sum_{j=1}^{2} \left(3 - j \right) \vartheta_{C,t+j} + \left(\mathbf{I}_{nk} - \mathbf{E}_t \right) \boldsymbol{\mathcal{B}}_{t+2} C_{t+1} \\ &\quad + \left(\mathbf{I}_{nk} - \mathbf{E}_t \right) \Big[\boldsymbol{\mathcal{B}}_{t+2} \boldsymbol{\mathcal{B}}_{t+1} + \boldsymbol{\mathcal{B}}_{t+1} \Big] \mathcal{Z}_t + \Gamma_{t+2} + \left(\mathbf{I}_{nk} + \boldsymbol{\mathcal{B}}_{t+2} \right) \Gamma_{t+1} \Bigg]. \end{aligned}$$

At $h = 3$, repeating these steps results in

$$\begin{aligned} \Delta e_{t+3} - \mathbf{E}_t \Delta e_{t+3} &= s_{\Delta e} \Big[C_{t+3} - C_t + \left(\mathbf{I}_{nk} - \mathbf{E}_t \right) \Big[\boldsymbol{\mathcal{B}}_{t+3} C_{t+2} + \boldsymbol{\mathcal{B}}_{t+3} \boldsymbol{\mathcal{B}}_{t+2} C_{t+1} \Big] \\ &\quad + \left(\mathbf{I}_{nk} - \mathbf{E}_t \right) \boldsymbol{\mathcal{B}}_{t+3} \boldsymbol{\mathcal{B}}_{t+2} \boldsymbol{\mathcal{B}}_{t+1} \mathcal{Z}_t + \Gamma_{t+3} + \boldsymbol{\mathcal{B}}_{t+3} \Gamma_{t+2} + \boldsymbol{\mathcal{B}}_{t+3} \boldsymbol{\mathcal{B}}_{t+2} \Gamma_{t+1} \Big], \end{aligned}$$

and

$$\begin{aligned} e_{t+3} - \mathbf{E}_t e_{t+3} &= s_{\Delta e} \Bigg[\sum_{j=1}^{3} \left(4 - j \right) \vartheta_{C,t+j} + \left(\mathbf{I}_{nk} - \mathbf{E}_t \right) \Big[\boldsymbol{\mathcal{B}}_{t+3} C_{t+2} + \boldsymbol{\mathcal{B}}_{t+3} \boldsymbol{\mathcal{B}}_{t+2} C_{t+1} \\ &\quad + \boldsymbol{\mathcal{B}}_{t+2} C_{t+1} \Big] + \left(\mathbf{I}_{nk} - \mathbf{E}_t \right) \Big[\boldsymbol{\mathcal{B}}_{t+3} \boldsymbol{\mathcal{B}}_{t+2} \boldsymbol{\mathcal{B}}_{t+1} + \boldsymbol{\mathcal{B}}_{t+2} \boldsymbol{\mathcal{B}}_{t+1} + \boldsymbol{\mathcal{B}}_{t+1} \Big] \mathcal{Z}_t \\ &\quad + \Gamma_{t+3} + \left(\mathbf{I}_{nk} + \boldsymbol{\mathcal{B}}_{t+3} \right) \Gamma_{t+2} + \left(\mathbf{I}_{nk} + \boldsymbol{\mathcal{B}}_{t+3} \boldsymbol{\mathcal{B}}_{t+2} + \boldsymbol{\mathcal{B}}_{t+2} \right) \Gamma_{t+1} \Bigg]. \end{aligned}$$

We rely on the previous equations and inductive reasoning to write the h-month ahead forecast error of the exchange rate as

$$\begin{aligned} e_{t+h} - \mathbf{E}_t e_{t+h} &= s_{\Delta e}\Bigg[\sum_{j=1}^{h}\Big(h+1-j\Big)\vartheta_{C,t+j} + \Big(\mathbf{I}_{nk} - \mathbf{E}_t\Big)\Bigg[\sum_{j=1}^{h-1}\boldsymbol{\mathcal{B}}_{t+j+1}C_{t+j} + \prod_{j=1}^{h-1}\boldsymbol{\mathcal{B}}_{t+j+1}C_{t+1}\Bigg] \\ &+ \Big(\mathbf{I}_{nk} - \mathbf{E}_t\Big)\sum_{j=1}^{h}\left(\prod_{\ell=1}^{j}\boldsymbol{\mathcal{B}}_{t+\ell}\right)\mathcal{Z}_t + \sum_{j=1}^{h}\Gamma_{t+j} + \sum_{j=1}^{h-1}\left(\sum_{\ell=j}^{h-1}\boldsymbol{\mathcal{B}}_{t+\ell+1}\right)\Gamma_{t+j}\Bigg], \end{aligned}$$

where $h \geq 2$.

We invoke the AUM with respect to the $\boldsymbol{\mathcal{B}}_{t+j}$s. This yields a local approximation of the previous equation for $h = 1$, $e_{t+1} - \mathbf{E}_t e_{t+1} \approx s_{\Delta e}\Big[\vartheta_{C,t+1} + \Gamma_{t,1}\Big]$, and for $h \geq 2$

$$e_{t+h} - \mathbf{E}_t e_{t+h} \approx s_{\Delta e}\Bigg[\sum_{j=1}^{h}\Big(h+1-j\Big)\vartheta_{C,t+j} + \sum_{j=1}^{h}\Gamma_{t,j} + \sum_{j=1}^{h-1}\boldsymbol{\mathcal{B}}_t^{h-j}\Gamma_{t,j}\Bigg], \tag{A7.2}$$

where $\Gamma_{t,j} \equiv \Big[\Big(\mathbf{A}_t^{-1}\boldsymbol{\Sigma}_{t,j}\,\eta_{t+j}\Big)' \;\mathbf{0}_{1\times n}\;\ldots\;\mathbf{0}_{1\times n}\Big]'$ and $\boldsymbol{\Sigma}_{t,j} \equiv \boldsymbol{\Sigma}_t \exp\left(\prod_{i=1}^{j}\xi_{t+i}\right)$ because the SVs are independent geometric random walks. The h-month ahead forecast error of e_t in equation (A7.2) is driven by innovations to the multivariate random walks of C_t and SV in Γ_t and the TVPs in $\boldsymbol{\mathcal{B}}_t$. The innovations to the TVP intercepts and SVs have declining weights moving away from the forecast horizon h. The latter weights are falling in powers of the TVP lag coefficients, which reflect the persistence in these drifting parameters.

Squaring equation (A7.2) produces our version of the Cogley and Sargent (2015) uncertainty statistic of e_t, $\mathcal{V}_t\left(e_{t+h} - \mathbf{E}_t e_{t+h}\right)$. For $h \geq 2$, this operation yields

$$\begin{aligned} \mathcal{V}_t\left(e_{t+h} - \mathbf{E}_t e_{t+h}\right) &\approx \sum_{j=1}^{h}\Big(h+1-j\Big)^2 s_{\Delta e}\mathbf{E}_t\left\{\vartheta_{C,t+j}\vartheta_{C,t+j}'\right\}s_{\Delta e}' + s_{\Delta e}\sum_{j=1}^{h}\mathbf{E}_t\left\{\Gamma_{t,j}\Gamma_{t,j}'\right\}s_{\Delta e}' \\ &+ s_{\Delta e}\sum_{j=1}^{h-1}\boldsymbol{\mathcal{B}}_t^{h-j}\mathbf{E}_t\left\{\Gamma_{t,k}\Gamma_{t,k}'\right\}\left(\boldsymbol{\mathcal{B}}_t^{h-j}\right)' s_{\Delta e}'. \end{aligned}$$

Hence, $\mathcal{V}_t\left(e_{t+1}-e_t\right)=s_{\Delta e}\left[\boldsymbol{\Omega}_{C,\vartheta}+\boldsymbol{\Omega}_{\Gamma,t,1}\right]s'_{\Delta e}$ and otherwise for $h\geq 2$

$$\mathcal{V}_t\left(e_{t+h}-\mathbf{E}_t e_{t+h}\right)\approx s_{\Delta e}\left[\frac{h(h+1)(2h+1)}{6}\boldsymbol{\Omega}_{C,\vartheta}+\sum_{j=1}^{h}\boldsymbol{\Omega}_{\Gamma,t,j}+\sum_{j=1}^{h-1}\boldsymbol{\mathcal{B}}_t^{h-j}\,\boldsymbol{\Omega}_{\Gamma,t,j}\left(\boldsymbol{\mathcal{B}}_t^{h-j}\right)'\right]s'_{\Delta e},\quad\text{(A7.3)}$$

where the lack of cross-products is because the innovations ϑ_{t+j} and ξ_{t+j} are uncorrelated at all leads and lags, the date t information set includes $\boldsymbol{\mathcal{B}}_t$, and $\boldsymbol{\Omega}_{C,\vartheta}=\mathbf{E}_t\left\{\vartheta_{C,t+j}\,\vartheta'_{C,t+j}\right\}$ and $\boldsymbol{\Omega}_{\Gamma,t,\ell}=\mathbf{E}_t\left\{\Gamma_{t,\ell}\,\Gamma'_{t,\ell}\right\}$ are $nk\times nk$ matrices full of zeros except the former has an upper right $n\times n$ block that is the lower left $n\times n$ block of $\boldsymbol{\Omega}_{\vartheta}$ and the latter has an upper right $n\times nk$ block that rearranges elements of $\mathbf{A}_t^{-1}\boldsymbol{\Sigma}_{t,j}\boldsymbol{\Sigma}'_{t,j}\left(\mathbf{A}_t^{-1}\right)'=\left(\mathbf{A}_t^{-1}\right)^j\boldsymbol{\Sigma}_t\,\mathbf{E}_t\left\{\exp\left(\prod_{k=1}^{j}\xi_{t+k}\xi'_{t+k}\right)\right\}\boldsymbol{\Sigma}'_t\left(\left(\mathbf{A}_t^{-1}\right)^j\right)'$ $=\left(\mathbf{A}_t^{-1}\right)^j\boldsymbol{\Sigma}_t\exp\left(j\,\boldsymbol{\Omega}_{\xi}\right)\boldsymbol{\Sigma}'_t\left(\left(\mathbf{A}_t^{-1}\right)^j\right)'$. Also, the sum $\sum_{j=1}^{h}(h+1-j)^2$ is easily shown to equal $h(h+1)^2-2(h+1)\sum_{j=1}^{h}j+\sum_{j=1}^{h}j^2$. The sums of the indexes are well known to be $\sum_{i=j}^{h}j=0.5h(h+1)$ and $\sum_{j=1}^{h}j^2=h(h+1)(2h+1)\big/6$, which gives $\sum_{i=0}^{h}(h+1-j)^2=h(h+1)(2h+1)\big/6$. Equation (A7.3) shows uncertainty in e_t depends on the innovation covariance matrix of the TV intercepts and the time-varying covariance matrix of the errors of the reduced-form VAR(k) weighted by powers of the companion matrix of the lag TVPs.

We sum the results of equations (A7.1) and (A7.3) and take the square root to measure instability in the *GBP*- and *USD-tael* nominal exchange rates. This is the instability statistic $\sqrt{\mathcal{V}_t\left(e_{t+h}-\mathbf{E}_t e_{t+h}\right)+\left(\mathbf{E}_t e_{t+h}-e_t\right)^2}$. Instability in p_t, which is the Shanghai-U.K. or Shanghai-U.S. WPI differential, is computed by substituting s_{π} for $s_{\Delta e}$ in equations (A7.1) and (A7.3). This yields the instability statistic $\sqrt{\mathcal{V}_t\left(p_{t+h}-\mathbf{E}_t p_{t+h}\right)+\left(\mathbf{E}_t p_{t+h}-p_t\right)^2}$.

A8. Additional Results

This section discusses median TV-impulse response functions (IRFs) and TV-forecast error vari-

ance decompositions (FEVDs) computed on posterior distributions of the TVP-SV-SVAR(2)-BL, our priors, and the China-U.K. sample $\left(\mathcal{Y}_{CUK,1:T}\right)$ or the China-U.S. sample $\left(\mathcal{Y}_{CUS,1:T}\right)$ from 1912M04 to 1934M09. Posterior median TV-IRFs (TV-FEVDs) are plotted in figures A5 to A8 (A13 to A16) on $\mathcal{Y}_{CUK,1:T}$. Figures A9 to A12 (A17 to A20) display posterior median TV-IRFs (TV-FEVDs) on $\mathcal{Y}_{CUS,1:T}$. Plots of the posterior medians of TV-IRFs and TV-FEVDs of i_t, p_t, ρ_t, and e_t are with respect to the international financial, cross-country demand, risk premium, and trend exchange rate, $\tau_{e,t}$, shocks moving from left to right in the top row and then the bottom row in figures A5 to A20. The IRFs and FEVDs of p_t and e_t are calculated by accumulating IRFs and FEVDs of π_t and Δe_t.

There is substantial time-variation in the posterior median IRFs of p_t and e_t to the four shocks in figures A6 and A8 and A10 and A12 on $\mathcal{Y}_{CUK,1:T}$ and $\mathcal{Y}_{CUS,1:T}$, respectively. The posterior median IRFs of i_t exhibit the most time with respect to the China-U.K. and China-U.S. risk premium shocks in figures A5 and A9. Figure A7 display posterior median IRFs of ρ_t that have more time-variation to the cross-country demand and $\tau_{e,t}$ China-U.K. shocks compared with the international financial and risk premium shocks. Add to this the China-U.S. international financial shock for the posterior median IRFs of ρ_t in figure A11.

Figures A13 to A20 show the posterior medians TV-FEVDs of i_t, π_t, and ρ_t are dominated by own shocks. These are the China-U.K. and China-U.S. international financial, cross-country demand, and risk premium shocks tied to i_t, π_t, and ρ_t, respectively, but these own posterior median FEVDs are declining over time. Furthermore, only figure A17 depicts the posterior median TV-FEVD of i_t with respect to the China-U.S. cross-country demand shock crossing the 20% threshold from the end of the First World War to the Great Depression.

Posterior median TV-FEVDs of $e_{GBP/S,1:T}$ and $e_{USD/S,1:T}$ are driven by the cross-country

demand and $\tau_{e,t}$ shocks in figures A16 and A20. The cross-country demand and $\tau_{e,t}$ shocks contribute between 35 to 50% to the variation of these posterior median TV-FEVDs from 1912M04 to 1934M09. At the end of the sample, the contribution is about 40% for each shock to movements in the posterior median TV-FEVDs of $e_{GBP/S,t}$. The split is closer to 50-50 for the posterior median TV-FEVDs of $e_{USD/S,t}$ at the same time. The implication is the international financial and risk premium shocks offer little to explain the variation of the posterior median TV-FEVDs of $e_{GBP/S,1:T}$ and $e_{USD/S,1:T}$ throughout the sample.

References

Amisano, G., C. Giannini (1997). Topics in Structural VAR Econometrics, 2nd Edition, Berlin, Germany: Springer.

Bacchiocchi, E., T. Kitagawa (2021). A note on global identification in structural vector autoregressions. CeMMAP working paper CWP03/21, The Institute for Fiscal Studies, Department of Economics, University College London.

Beveridge, S., C.R. Nelson (1981). A new approach to decomposition of economic time series into permanent and transitory components with particular attention to measurement of the 'business cycle'. *Journal of Monetary Economics* 7, 151–174.

Bratter, H.M. (1933). The monetary use of silver in 1933. Trade Promotion Series, No. 149, Department of Commerce. Washington, D.C.: U.S. Government Printing Office.

Burns, A.F., W.C. Mitchell (1946). Measuring Business Cycle. New York: NY: National Bureau of Economic Research.

Canova, F., F.J. Pérez Forero (2015a). Estimating overidentified, non-recursive, time varying coefficient structural VARs. *Quantitative Economics* 6, 359–384.

Canova, F., F.J. Pérez Forero (2015b). Supplement to "Estimating overidentified, non-recursive, time varying coefficient structural VARs." available at `https://onlinelibrary.wiley.com/action/downloadSupplement?doi=10.3982%2FQE305&file=quan116-sup-0001-Supplement.pdf`

Chow, G.C., A-L. Lin (1971). Best linear unbiased interpolation, distribution, and extrapolation of time series by related series. *Review of Economics and Statistics* 53, 372–375.

Cogley, T., G.E. Primiceri, T.J. Sargent (2010). Inflation-Gap Persistence in the US. *American Economic Journal: Macroeconomics* 2, 43–69.

Cogley, T., T.J. Sargent (2015). Measuring price-level uncertainty and instability in the United States, 1850–2012. *Review of Economics and Statistics* 97, 827–838.

Cogley, T., A.M. Sbordone (2008). Trend inflation, indexation, and inflation persistence in the New Keynesian Phillips curve. *American Economic Review* 98, 2101–2126.

Dean, A. (2020). China and the End of Global Silver, 1873–1937. Ithaca, NY: Cornell University Press.

Elliott, G., T.J. Rothenberg, J.H. Stock (1996). Efficient tests for an autoregressive unit root. *Econometrica* 64, 813–836.

El-Shagi, L. Zhang (2020). Trade effects of silver price fluctuations in 19th-century China: A macro approach. *China Economic Review* 63, 101522.

Engel, C. (2016). Exchange rates, interest rates, and the risk premium. *American Economic Review* 106, 436–474.

Hamilton, J.D. (1994). Time Series Analysis. Princeton, NJ: Princeton University Press.

Harvey, A., E. Ruiz, N. Shephard (1994). Multivariate stochastic variance models," *Review of Economic Studies* 61, 247–264.

Ho, T-K., C-C. Lai (2016). A silver lifeboat, not silver fetters: Why and how the silver standard insulated China from the 1929 Great Depression. *Journal of Applied Econometrics* 31, 403–419.

Hodrick, R.J. (1992). Dividend yields and expected stock returns: Alternative procedures for inference and measurement. *Review of Financial Studies* 5, 357–386.

Jacks, D.S., S. Yan, L. Zhao (2017). Silver points, silver flows, and the measure of Chinese financial integration. *Journal of International Economics* 108, 377–386.

Kong, M. (ed.) (1988). *Nankai Jingji Zhishu Ziliao Huibian* (Nankai Economic Indicators). Beijing, China: Chinese Academy of Social Sciences.

Kreps, D. (1998). Anticipated utility and dynamic choice. In Frontiers of Research in Economic Theory: Nancy L. Schwartz Memorial Lectures, 1983–1997. Jacobs, D.P., E. Kalai, M.I. Kamien, N.L. Schwartz (eds.), 242–274, Cambridge, UK: Cambridge University Press.

Leavens, D.H. (1939). Silver Money. Cowles Commission for Research in Economics, Monograph no. 4. Bloomington, IN: Principia Press, Inc.

Ma, D. (2012). Money and monetary system in China in the 19th–20th Century: An overview. Working papers no. 159, Department of Economic History, London School of Economics.

Ma, D. (2017). The rise of a financial revolution in Republican China in 1900–1937: An institutional narrative. Working paper no. 319, Department of Economics, University of Warwick.

Ma, D. (2019). Financial revolution in Republican China during 1900–37: A survey and a new interpretation. *Australian Economic History Review* 59, 242–262.

Ma, D., L. Zhao (2020). A silver transformation: Chinese monetary integration in times of political disintegration, 1898–1933. *Economic History Review*, 73, 513–539.

MacKinnon, J.G. (1994). Approximate asymptotic distribution functions for unit-root and cointegration bootstrap. *Journal of Business and Economic Statistics* 12, 167–176.

MacKinnon, J.G. (1996). Numerical distribution functions for unit root and cointegration tests. *Journal of Applied Econometrics* 11, 601–618.

MacKinnon, J.G. (2010). Critical values for cointegration tests. QED wp-1227, Department of Economics, Queen's University, Kingston, Ont., Canada, available at `https://www.econ.queensu.ca/sites/econ.queensu.ca/files/wpaper/qed_wp_1227.pdf`..

Nason, J.M., G.W. Smith (2023). UK inflation dynamics since the thirteenth century. *International Economic Review* 64, 1595–1614.

Omori, Y., S. Chib, N. Shephard, J. Nakajima (2007). Stochastic volatility with leverage: Fast and efficient likelihood inference. *Journal of Econometrics* 140, 425–449.

Palma, N., L. Zhao (2021). The efficiency of the Chinese silver standard, 1920–1933. *Journal of Economic History* 81, 872–908.

Pan, Q., D. Long (2015). A study of the IOR of Shanghai Qianzhuang in the early 20th century: Based on the historical materials of Shanghai Qianzhuang. *Jing Ji Yan Jiu* (*Contemporary Economic Research*) 2, 160–171.

Rothenberg, T.J. (1971). Identification in parametric models. *Econometrica* 39, 577–591.

Rubio-Ramírez, J.F., D.F. Waggoner, T. Zha (2010). Structural vector autoregressions: Theory of identification and algorithms for inference. *Review of Economic Studies* 77, 665–696.

Shanghai Research Institute of Economics, Chinese Academy of Sciences and Research Institute of Economics, Shanghai Social Sciences Academy (1958). *Shanghai chieh-fang chien-hou we-chia tzu-liao hui-pien* (A Collection of Data on Prices in Shanghai before and after Liberation), 1921–1957. Shanghai, China: Shanghai People's Publishing House.

Silber, W.L. (2019). The Story of Silver: How the White Metal Shaped America and the Modern World. Princeton, NJ: Princeton University Press.

Wu, D. (1935). *Yige xinde waihui zhishu* (A new exchange rate index). *Review of Political Economy* 21, 463–509.

Young, J.P. (1931). The Shanghia *tael*. *American Economic Review* 21, 682–684.

Zhongguo ren min yin hang Shanghai Shi fen hang (People's Bank of China, Shanghai Branch) (1960). *Shanghai qianzhuang shiliao* (Shanghai Banking Historical Records). Shanghai, China: Shanghai People's Press.

Table A1. Business Cycle Dates for the U.K. and U.S., 1912m04–1934m09

U.K.		U.S.	
Peak	Trough	Peak	Trough
1912m12	1914m09	1913m01	1914m12
1918m10	1919m04	1918m08	1919m03
1920m03	1921m06	1920m01	1921m07
1924m11	1926m07	1923m05	1924m07
1927m03	1928m09	1926m10	1927m11
1929m07	1932m08	1929m08	1933m03

Notes: Table A1 of Burns and Mitchell (1946) is the source of the U.K. business cycle dates. The peak (trough) of the U.K. business cycle is the middle month of stage V (IX). Burns and Mitchell (1946, p. 29) define stage V as the part of the business cycle that "covers the three months centered on the peak." Similarly, stage IX is "the three months centered on the terminal trough." The U.S. business cycle dates are determined by the NBER. The NBER makes these dates available online at its website `https://www.nber.org/research/data/us-business-cycle-expansions-and-contractions`.

Table A2. Unit Root Tests on Shanghai, U.K., and U.S. Samples, 1912M04–1934M09

Variable	ADF	DF-GLS
$i_{S,t}$	-1.62	-0.93
	$\left(0.78\right)$	$\left(0.86\right)$
$i_{UK,t}$	-2.07	-2.60
	$\left(0.57\right)$	$\left(0.09\right)$
$i_{US,t}$	-1.33	-1.68
	$\left(0.88\right)$	$\left(0.47\right)$
$\pi_{S,t}$	-6.44	-6.26
	$\left(0.00\right)$	$\left(0.00\right)$
$\pi_{UK,t}$	-3.55	-3.54
	$\left(0.03\right)$	$\left(0.01\right)$
$\pi_{US,t}$	-3.19	-3.58
	$\left(0.09\right)$	$\left(0.01\right)$
$p_{S,t}$	-2.10	-1.88
	$\left(0.55\right)$	$\left(0.36\right)$
$p_{UK,t}$	-2.92	-1.05
	$\left(0.16\right)$	$\left(0.82\right)$
$p_{US,t}$	-2.22	-1.08
	$\left(0.48\right)$	$\left(0.80\right)$

Notes: The table presents t-ratios of augmented Dickey-Fuller (ADF) and Dickey-Fuller generalized least squares (DF-GLS) unit root tests. The parentheses contain asymptotic p-values. Small p-values indicate the null hypothesis of a unit root is not rejected. The t-ratios and p-values are computed using the *Python* (v.3.10.12) toolbox *arch* (v.6.3.0) and its commands `arch.unitroot.ADF` and `arch.unitroot.DFGLS`. These commands obtain asymptotic p-values from MacKinnon (1994, 2010). The ADF and DF-GLS regressions are estimated with a constant and linear time trend. The first significant t-ratio criterion is used to select the lag length of the first difference of the dependent variable in the ADF regression. Before estimating the DF-GLS regression the dependent variable is detrended using the OLS method recommended by the documentation of the `arch.unitroot.DFGLS` command. The lag length of the DF-GLS regression is chosen using the Akaike information criterion. The (maximum) lag length is 24 months for $i_{j,t}$ and $p_{j,t}$, but lowered to 18 months for $\pi_{j,t}$, $j = S, UK$, and US.

Table A3. Unit Root Tests on the $y_{CUK,1:T}$ and $y_{CUS,1:T}$ Samples and Nominal and Real Exchange Rates 1912M04–1934M09

	$y_{CUK,1:T}$		$y_{CUS,1:T}$	
Variable	ADF	DF-GLS	ADF	DF-GLS
$i_{S,t} - i_{j,t}$	−2.89	−2.69	−4.02	−8.72
	(0.16)	(0.08)	(0.01)	(0.00)
$\pi_{S,t} - \pi_{j,t}$	−4.79	−4.75	−4.10	−3.94
	(0.00)	(0.00)	(0.01)	(0.00)
$\rho_{\ell/S,t}$	−4.65	−7.16	−4.50	−8.36
	(0.00)	(0.00)	(0.00)	(0.00)
$\Delta e_{\ell/S,t}$	−4.10	−9.81	−3.56	−7.13
	(0.01)	(0.00)	(0.03)	(0.00)
$p_{S,t} - p_{j,t}$	−2.56	−1.08	−2.48	−1.61
	(0.30)	(0.80)	(0.33)	(0.52)
$e_{\ell/S,t}$	−1.98	−1.59	−2.49	−2.02
	(0.61)	(0.53)	(0.33)	(0.29)
$q_{\ell/S,t}$	−2.21	−3.67	−1.88	−1.77
	(0.48)	(0.00)	(0.66)	(0.42)

Notes: The table reports t-ratios and p-values that depend on (maximum) lag lengths of 12 months for $i_{S,t} - i_{j,t}$, $\pi_{S,t} - \pi_{j,t}$, $\rho_{\ell/S,t}$, and $\Delta e_{\ell/S,t}$ $j = UK$ or US and $\ell = GBP$ or USD. The ADF and DF-GLS regressions of $e_{\ell/S,t}$ and $q_{\ell/S,t}$ use a (maximum) lag lengths of 24 months. Otherwise, see the notes to table A1.

Table A4. Priors on the TVP-SV-SVAR(k)s

$$
\begin{aligned}
\mathbf{A}_t\, y_t &= \mathbf{A}_t\, \mathbf{c}_t + \mathbf{A}_t \sum_{\ell=1}^{k} \mathbf{B}_{\ell,t}\, y_{t-\ell} + \mathbf{\Gamma}_t \eta_t, && \eta_t \sim \mathcal{N}\big(\mathbf{0}, \mathbf{I}_n\big),\\
\mathbb{B}_{t+1} &= \mathbb{B}_t + \vartheta_{t+1}, && \vartheta_{t+1} \sim \mathcal{N}\big(\mathbf{0}, \mathbf{\Omega}_\vartheta\big),\\
a_{t+1} &= a_t + \psi_{t+1}, && \psi_{t+1} \sim \mathcal{N}\big(\mathbf{0}, \mathbf{\Omega}_\psi\big),\\
\ln y_{t+1}^2 &= \ln y_t^2 + \xi_{t+1}, && \xi_{t+1} \sim \mathcal{N}\big(\mathbf{0}, \mathbf{\Omega}_\xi\big).
\end{aligned}
$$

Initial SVAR Parameters	Prior Distributions	Parameters θ_1	Parameters θ_2
$\mathbb{B}_0$, Initial Intercept and Lags of VAR(k)	$\mathcal{MN}$	$\underline{\mathbb{B}}$	$\underline{\mathbf{\Omega}}_{\mathbb{B}}$
$\mathbf{\Omega}_\vartheta$, Covariance Matrix of Innovations to $\mathbb{B}_t$	$\mathcal{IW}$	$n(kn+1)$	$\kappa_{\mathbb{B}}\underline{\mathbf{\Omega}}_{\mathbb{B}}$
a_0, Initial Impact Coefficients of SVAR(k)	$\mathcal{MN}$	$\underline{a}$	$\underline{\mathbf{\Omega}}_a$
$\mathbf{\Omega}_\psi$, Covariance Matrix of Innovations to a_t	$\mathcal{IW}$	$\dim(a_t)+1$	$\kappa_a\underline{\mathbf{\Omega}}_a$
$\ln y_0^2$, Initial SV of SVAR(k)	$\mathcal{M}$-$\mathcal{LN}$	$\underline{y}^2$	$\kappa_y\underline{\mathbf{\Omega}}_y$
$\sigma_{j,\xi}^2$, Variance of Innovations to $\ln y_{j,t}^2$	$\mathcal{IG}$	1	$0.5\underline{\sigma}_\xi^2$

Notes: Parameters of the prior distributions are listed under the columns θ_1 and θ_2. We give the initial conditions, $\mathbb{B}_0$, of the intercepts and lag coefficients, $\mathbb{B}_t \equiv \text{vec}\Big(\big[\mathbf{B}_{1,t}, \ldots, \mathbf{B}_{k,t}, \ \mathbf{c}_t\big]\Big)$, of the TVP-SV-SVAR($k$)s a multivariate normal ($\mathcal{MN}$) prior, where $k = 2$. The prior mean is set to OLS estimates of the reduced-form VAR(k), on the China-U.K. and China-U.S. samples from 1912M04 to 1934M09. The covariance matrix of the prior, $\underline{\mathbf{\Omega}}_{\mathbb{B}}$, equals 0.25 of the OLS covariance matrix of these coefficients. The prior of the covariance matrix of innovations to $\mathbb{B}_t$ is $\mathbf{\Omega}_\vartheta \sim$ inverse-Wishart ($\mathcal{IW}$) with $n(nk+1)$ degrees of freedom and a scale matrix $\kappa_{\mathbb{B}}\underline{\Omega}_{\mathbb{B}}$, where $\kappa_{\mathbb{B}}$ is set to achieve 50 to 60% acceptance rates of non-explosive posterior draws for $\mathbb{B}_t$. Fixed coefficient SVAR(k)s are estimated by maximum likelihood (ML) on the China-U.K. and China-U.S. samples to recover the prior means $\underline{a}$ and $\underline{y}^2$ of the initial conditions a_0 and $\ln y_0^2$, where a_0 is the vector of off-diagonal non-zero elements of $\mathbf{A}_0$ and $\text{diag}(\mathbf{\Gamma}_0) \equiv y_0 = \big[y_{1,0} \ldots y_{n,0}\big]'$. The prior covariance matrix of a_0, $\underline{\Omega}_a$, is a matrix that has zeros in its off-diagonal elements and a diagonal containing the absolute values of $\underline{a}$. We place a $\mathcal{MN}$ prior a_0 parameterized by $\underline{a}$ and $\underline{\Omega}_a$. The covariance matrix $\mathbf{\Omega}_\psi$ of the innovations to its random walk generating equation has an $\mathcal{IW}$ prior with degrees of freedom equal to one plus the dimension of a_t and the scale matrix $\underline{\mathbf{\Omega}}_a$ multiplied by κ_a, which is selected to achieve acceptance rates in the Metropolis step of the MCMC of around 32% for posterior draws of a_t. The prior of the vector of initial SVs, $\ln y_0^2$, is endowed with a multivariate-log normal ($\mathcal{M}$-$\mathcal{LN}$) distribution parameterized by $\underline{y}^2$ and $\underline{\Omega}_y$, which is the ML covariance matrix of $\underline{y}^2$. The variance, $\sigma_{j,\xi}^2$, of the innovations to $\ln y_{j,t+1}^2$, $j = 1, \ldots, n$, has an inverse-gamma ($\mathcal{IG}$) prior with shape and scale parameters equal to one and half of $\underline{\sigma}_\xi^2 = 10^{-4}$. This prior is the same as drawing a (univariate) random variable distributed $\mathcal{IW}\left(2, \underline{\sigma}_\xi^2\right)$.

Figure A1: Nominal Short-Term Interest Rates for Shanghai, London, and New York City, 1912M04 to 1934M09

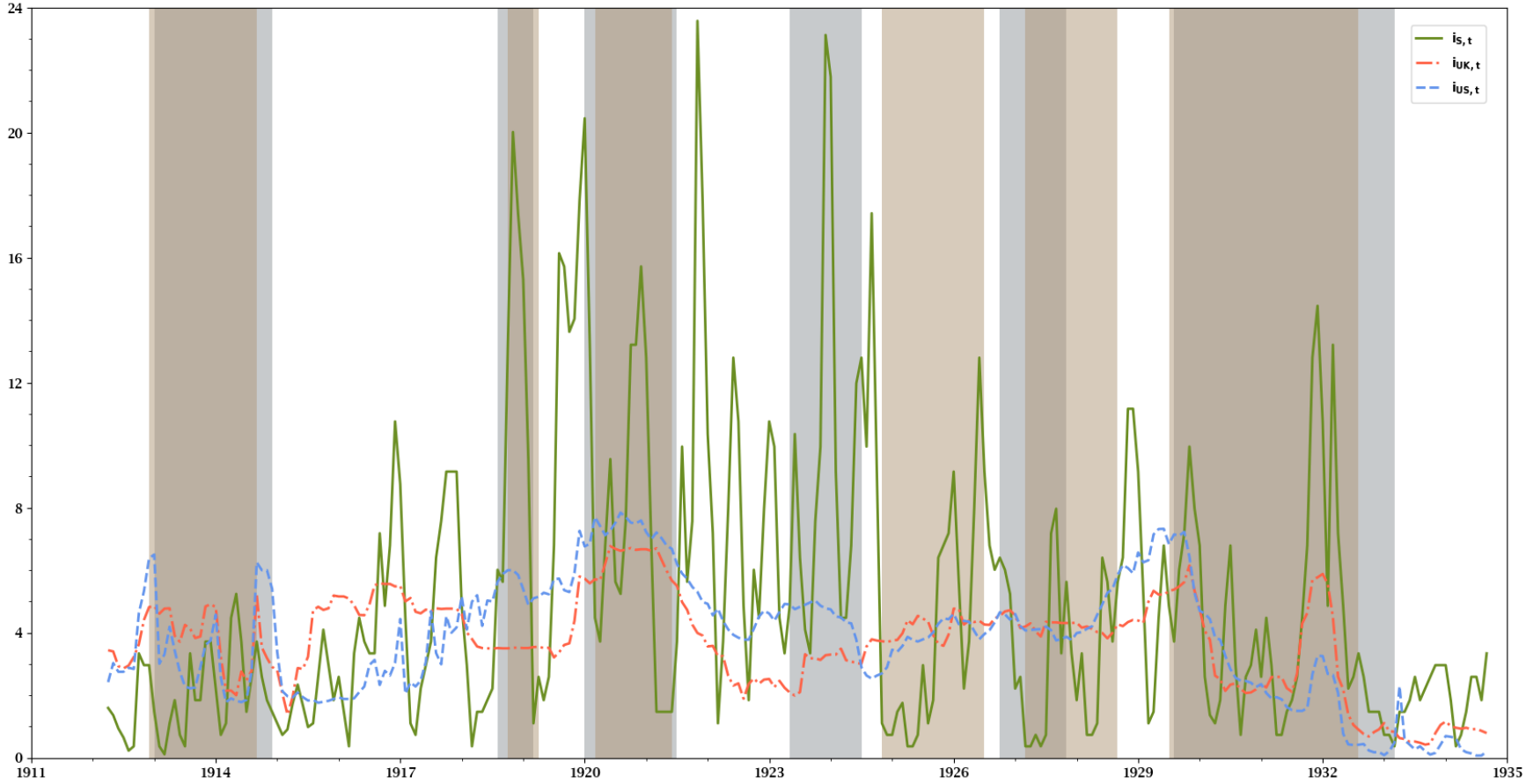

Notes: The figure plots nominal Shanghai, U.K., and U.S. interest rates, $i_{S,t}$, $i_{UK,t}$, and $i_{US,t}$. Tan (silver) shaded vertical bars are Burns-Mitchell (NBER) recession dates for the U.K. (U.S.); see table A1.

Figure A2: Log and Year over Year and Month over Month Inflation Shanghai, U.K, and U.S. WPIs, 1912M04 to 1934M09

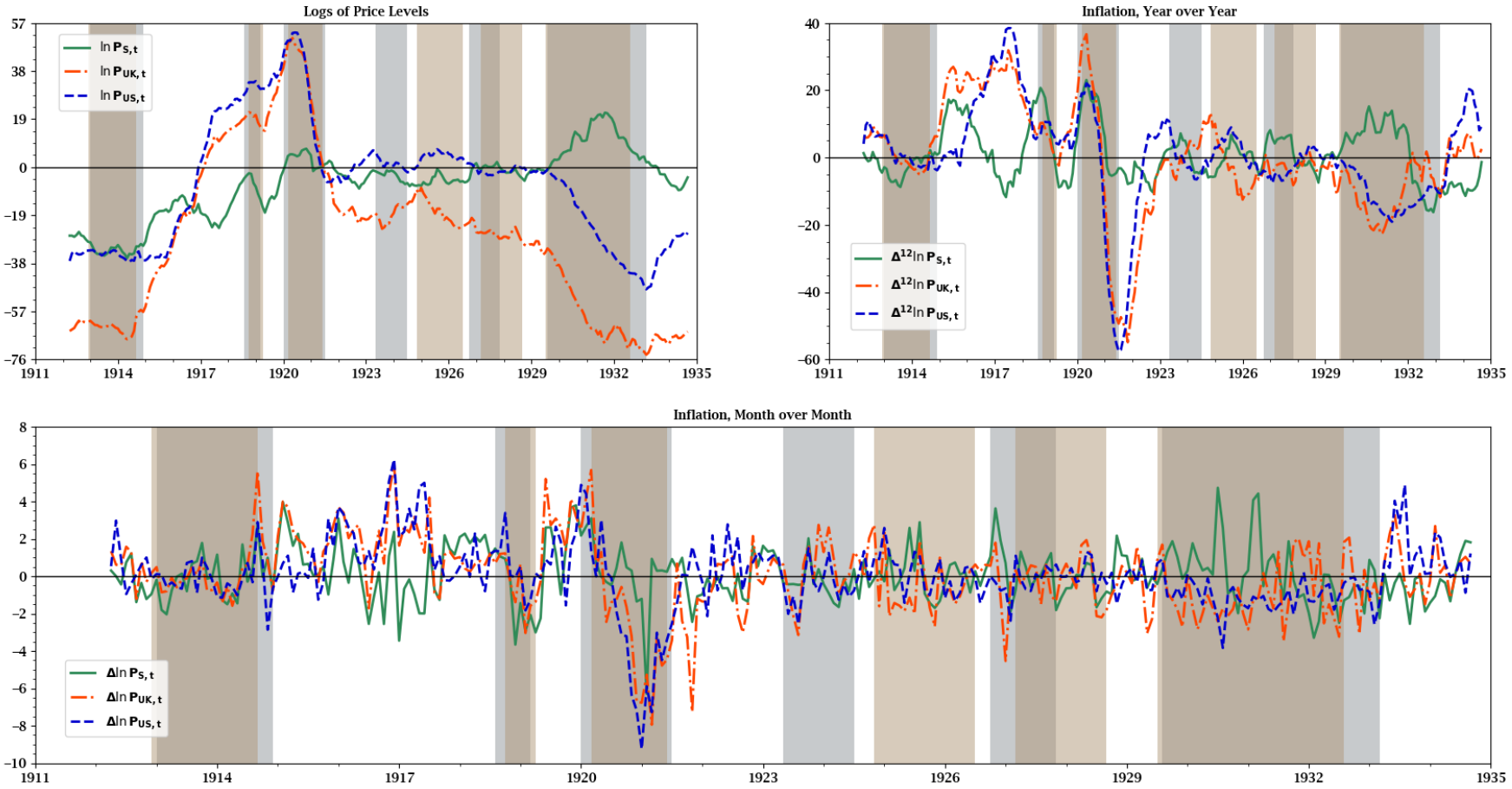

Notes: The top left panel plots 100 times the log of the price levels, $100p_{j,t}$, $j = S, UK, US$. Year over year inflation, $\Delta^{12}p_{j,t}$, is in the top right panel. The bottom panel displays month over month inflation, $\Delta p_{j,t}$. Tan (silver) shaded vertical bars are Burns-Mitchell (NBER) recession dates for the U.K. (U.S.); see table A1.

Figure A3: Log Levels of and Year over Year Returns on *GBP*-Shanghai *Tael* and *USD*-Shanghai *Tael* Nominal Exchange Rates, 1912M04 to 1934M09

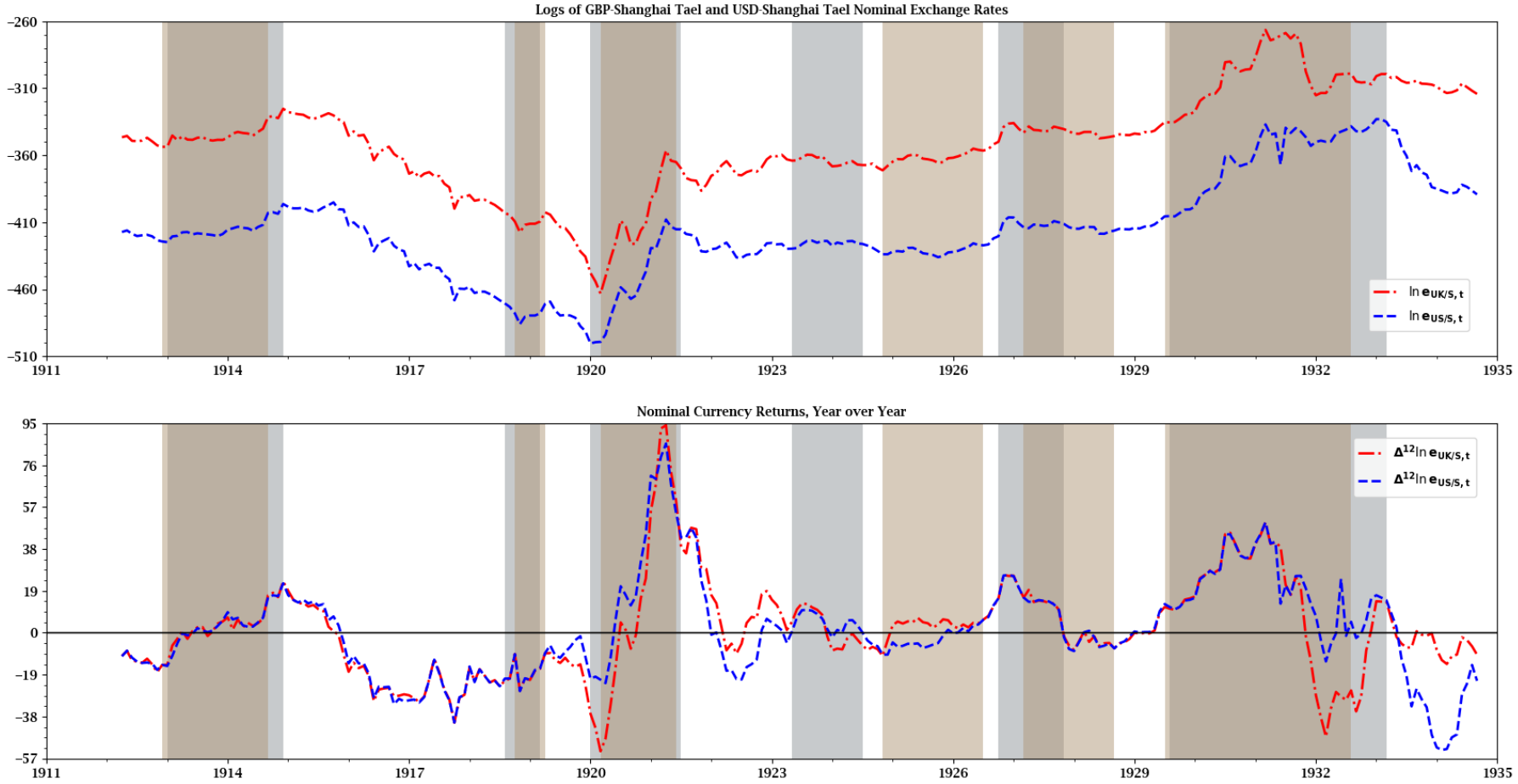

Notes: The top panel displays 100 times the log of the nominal exchange rates, $100e_{j/S}$, j = *GBP*, *USD*. Plots of year over year nominal currency returns, $\Delta^{12}e_{j/S,t}$, appear in the bottom panel. Tan (silver) shaded vertical bars are Burns-Mitchell (NBER) recession dates for the U.K. (U.S.); see table A1.

Figure A4: Log Levels and Year over Year and Month over Month Growth of *GBP*-Shanghai *tael* and *USD*-Shanghai *tael* Real Exchange Rates, 1912M04 to 1934M09

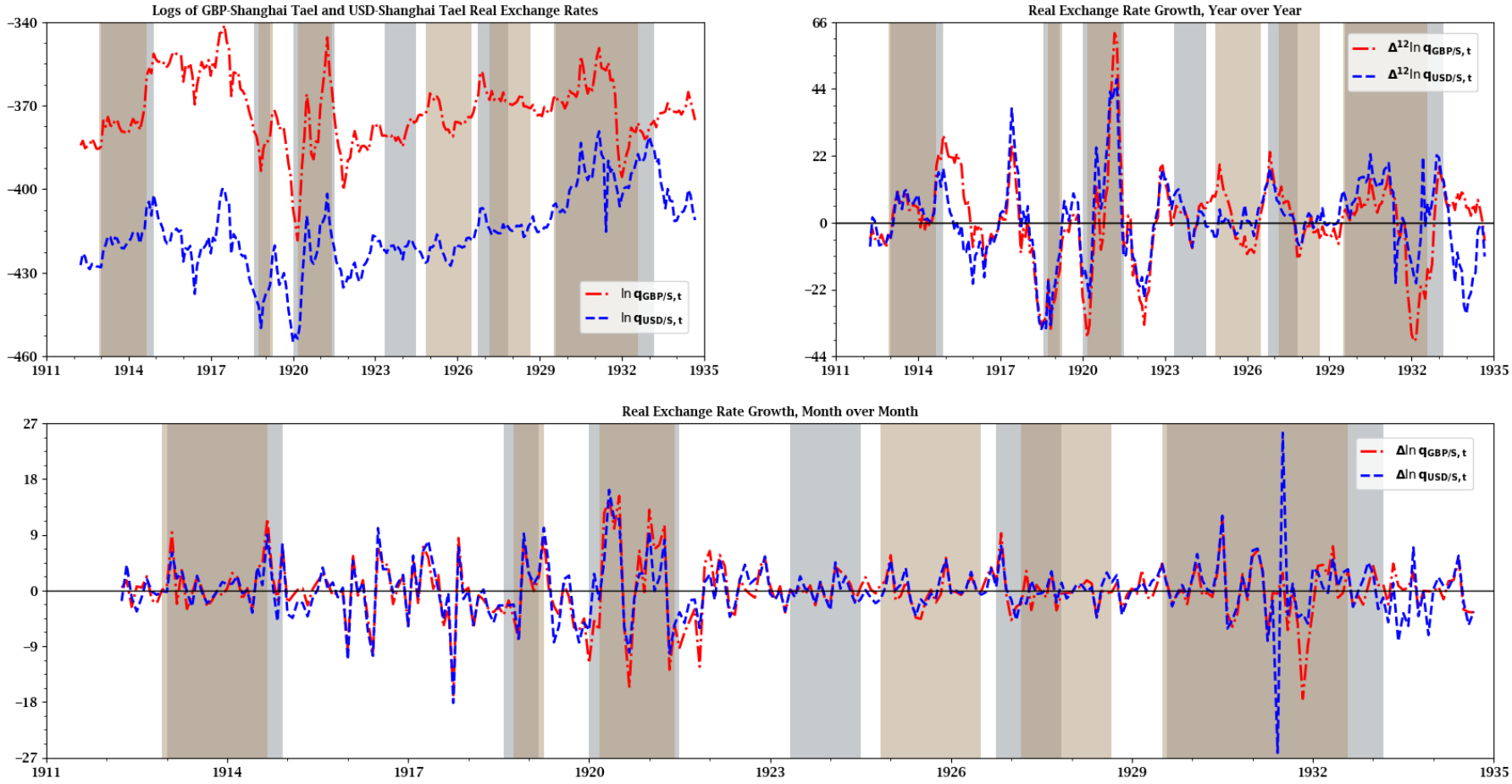

Notes: The top left panel plots 100 times the log of the real exchange rates, $100q_{j/S}$, $j = UK, US$. Year over year (month over month) real currency returns, $\Delta q_{j/S,t}$ $\left(\Delta^{12} q_{j/S,t}\right)$, appear in the top right (botttom) panel. Tan (silver) shaded vertical bars are Burn-Mitchell (NBER) recession dates for the U.K. (U.S.); see table A1.

Figure A5: Posterior Median IRFs of i_t on the China-U.K. Sample, 1912M04 to 1934M09

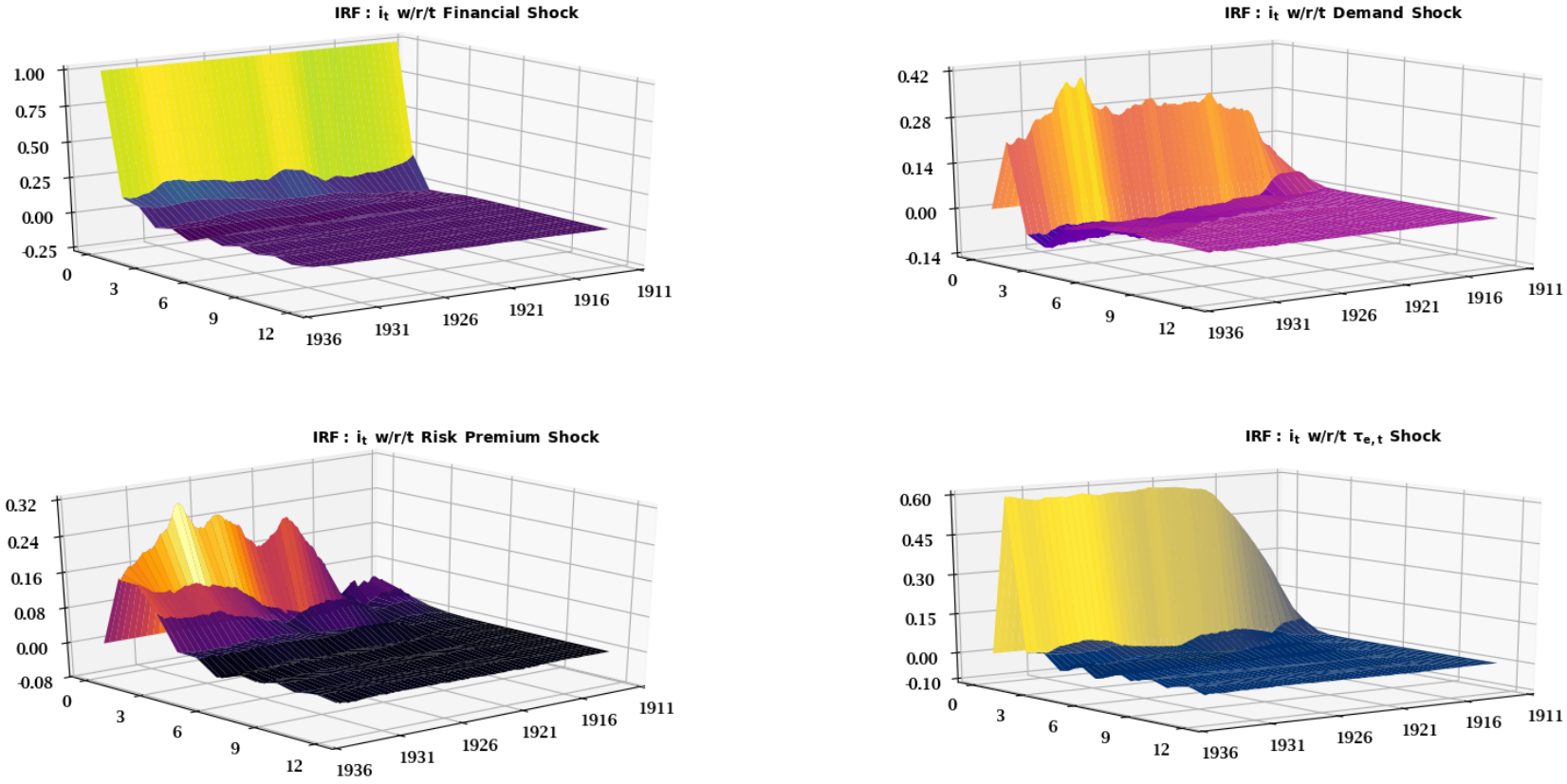

Notes: The median IRFs are computed on the posterior distribution of TVP-SV-SVAR(2)-BL conditional on $y_{CUK,1:T}$ and our priors.

Figure A6: Posterior Median IRFs of π_t on the China-U.K. Sample, 1912M04 to 1934M09

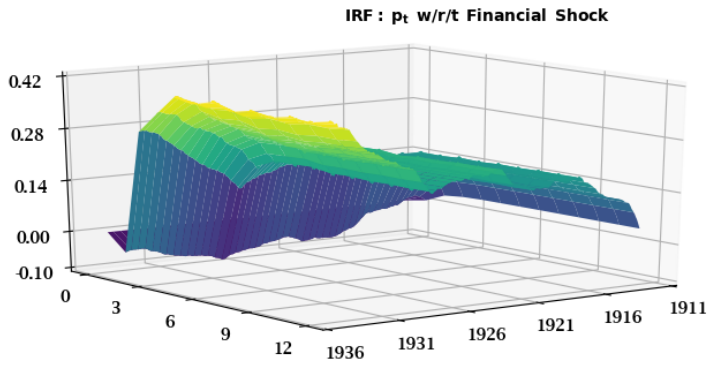

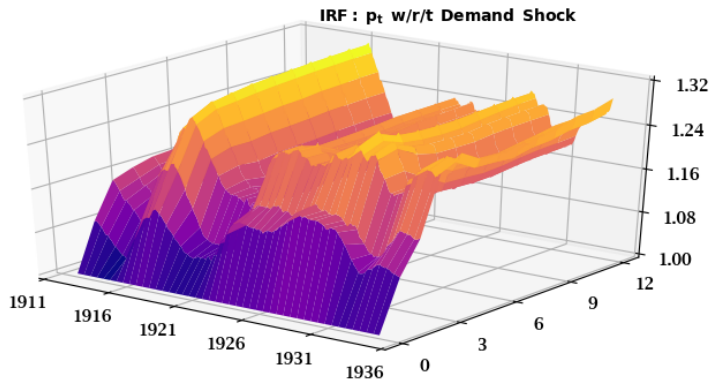

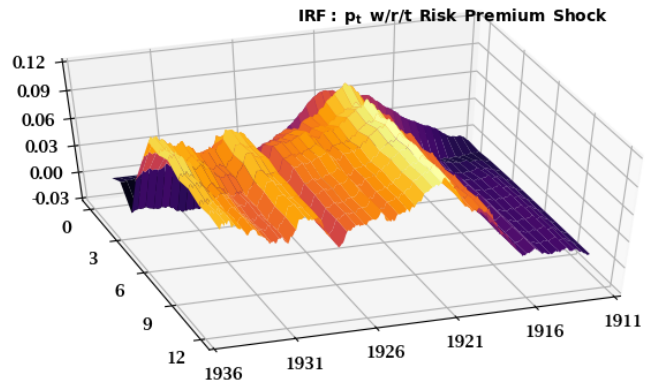

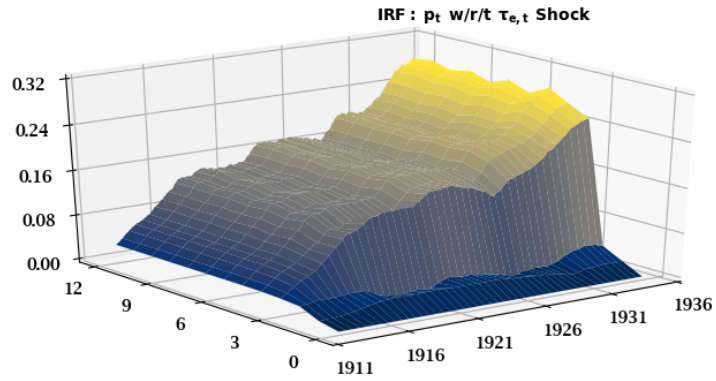

Notes: See the notes to figure A5.

Figure A7: Posterior Median IRFs of ρ_t on the China-U.K. Sample, 1912M04 to 1934M09

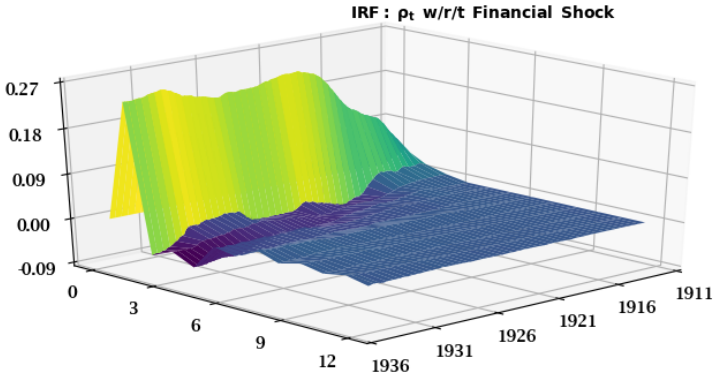

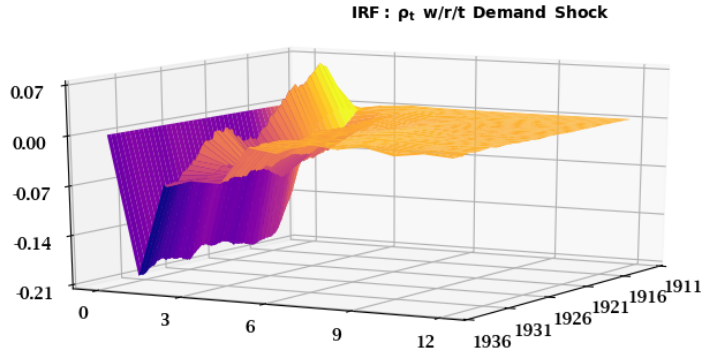

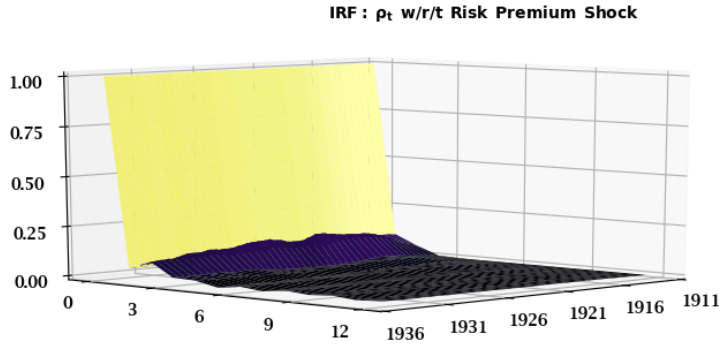

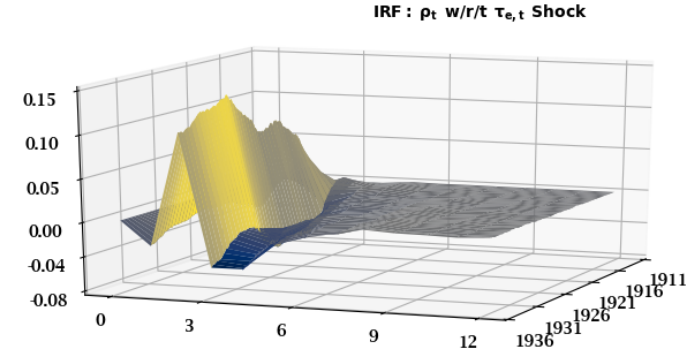

Notes: See the notes to figure A5.

Figure A8: Posterior Median IRFs of Δe_t on the China-U.K. Sample, 1912M04 to 1934M09

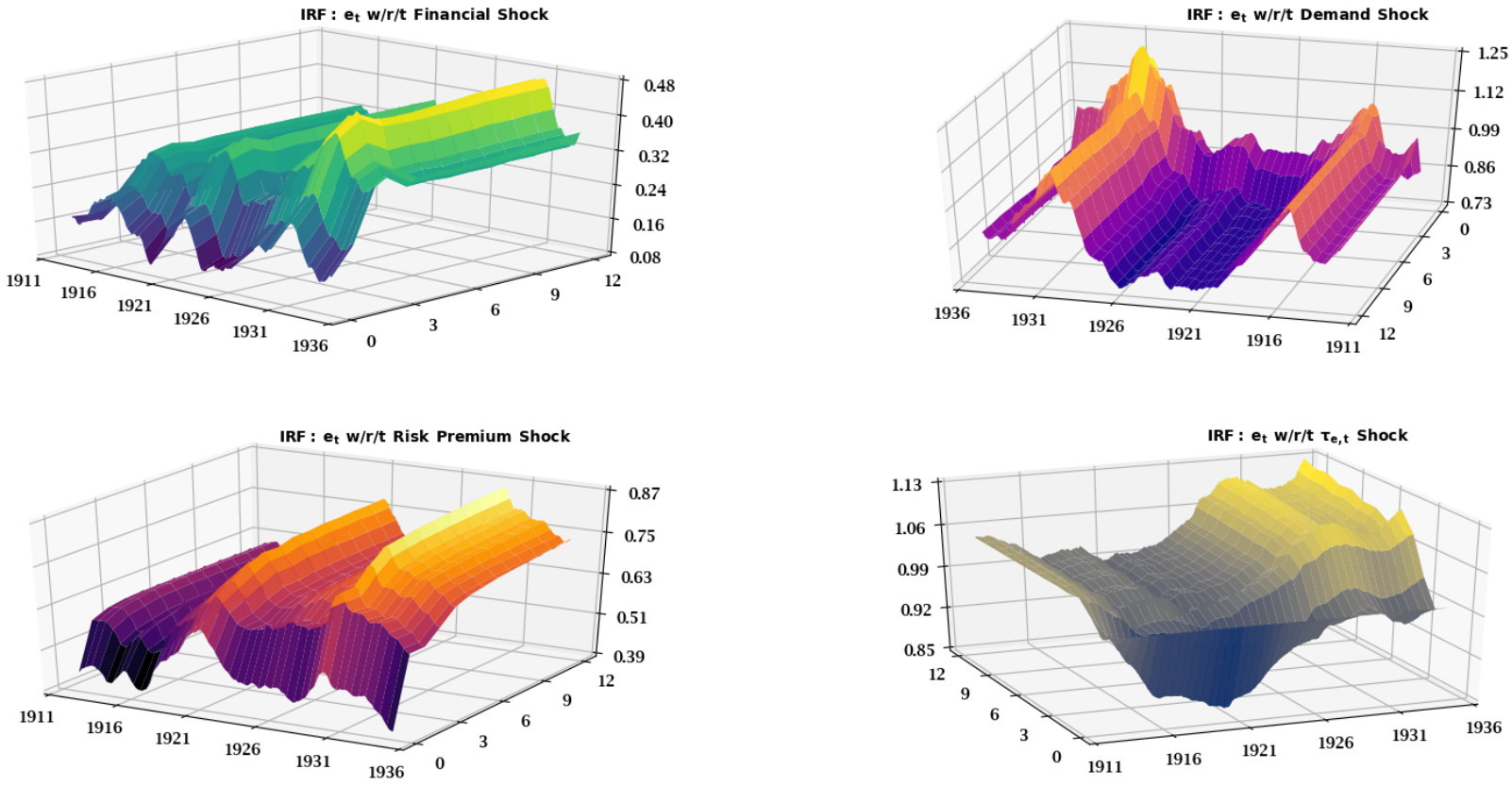

Notes: See the notes to figure A5.

Figure A9: Posterior Median IRFs of i_t on the China-U.S. Sample, 1912M04 to 1934M09

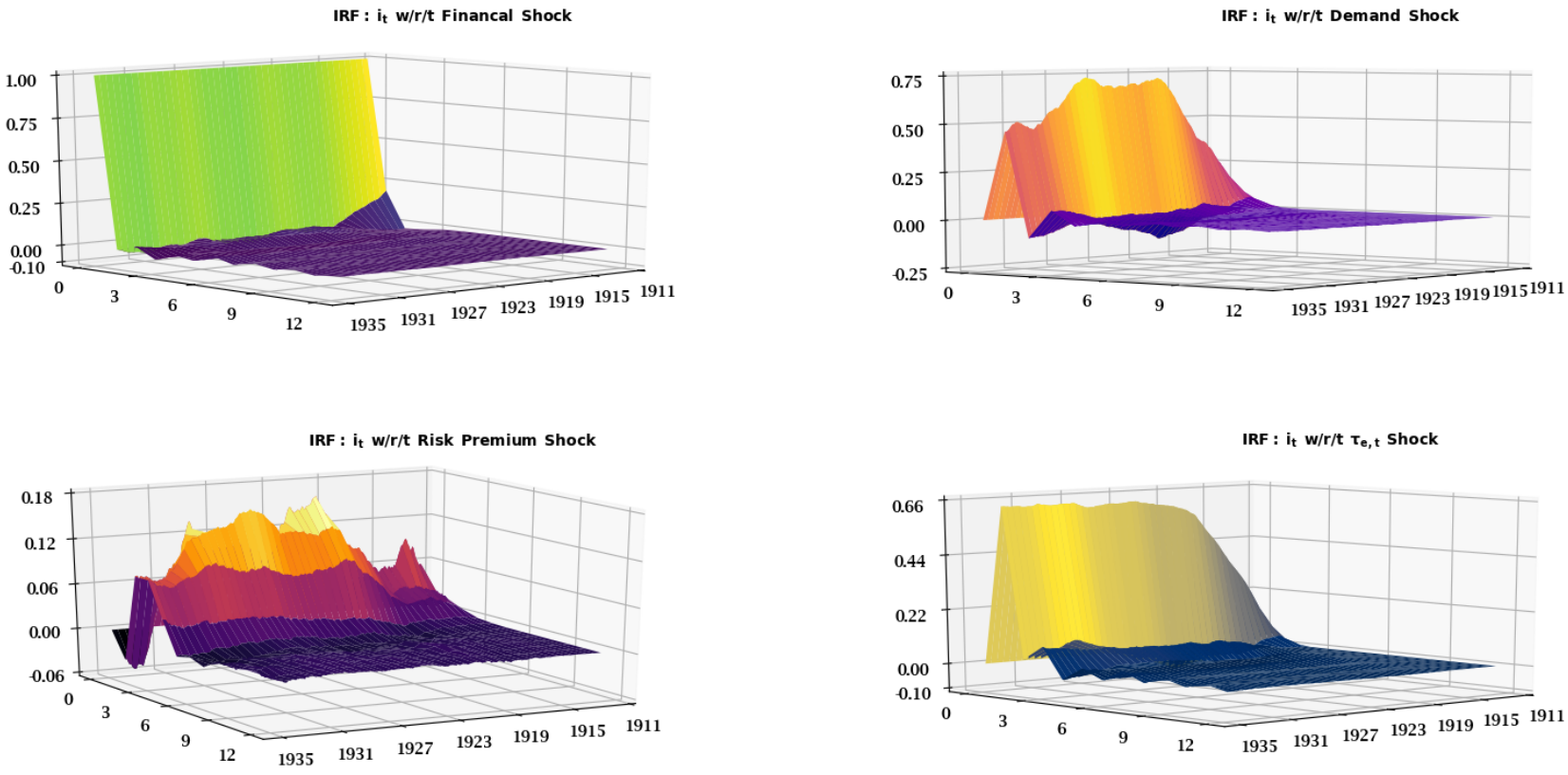

Notes: The median IRFs are computed on the posterior distribution of TVP-SV-SVAR(2)-BL conditional on $y_{CUS,1:T}$ and our priors.

Figure A10: Posterior Median IRFs of π_t on the China-U.S. Sample, 1912M04 to 1934M09

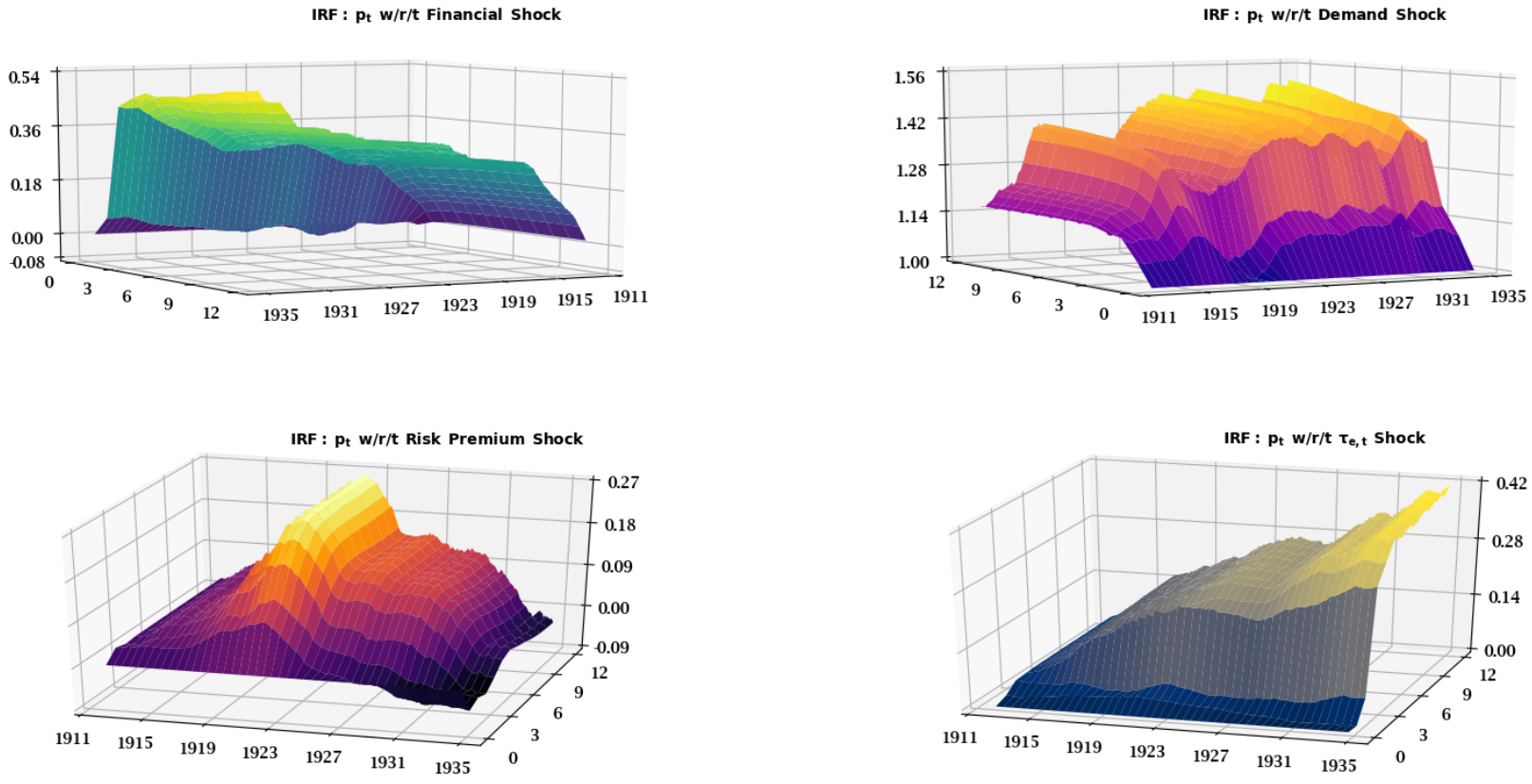

Notes: See the notes to figure A9.

Figure A11: Posterior Median IRFs of ρ_t on the China-U.S. Sample, 1912M04 to 1934M09

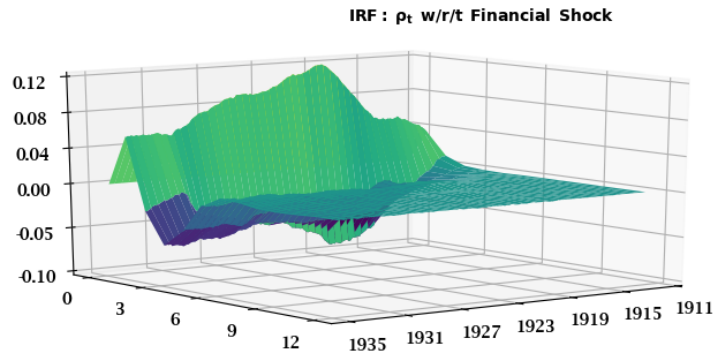

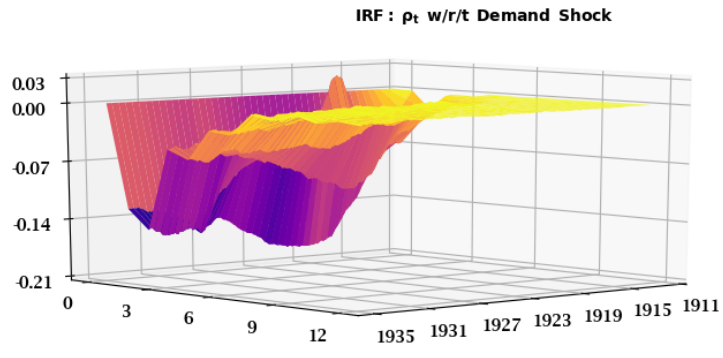

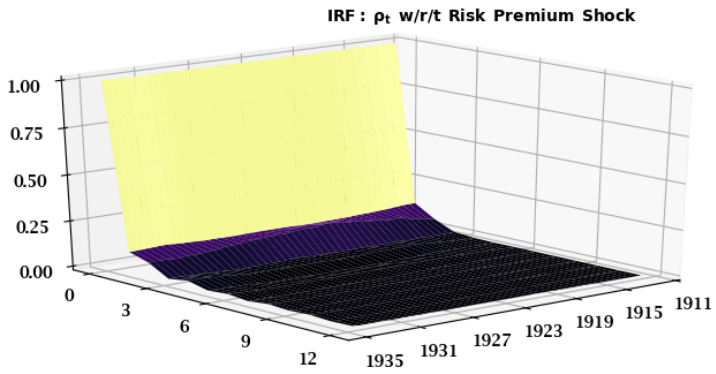

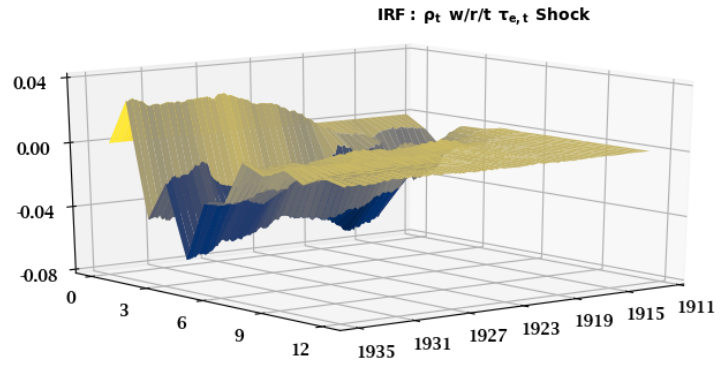

Notes: See the notes to figure A9.

Figure A12: Posterior Median IRFs of Δe_t on the China-U.S. Sample, 1912M04 to 1934M09

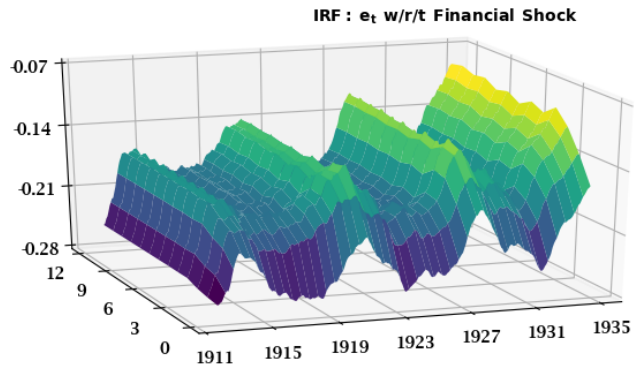

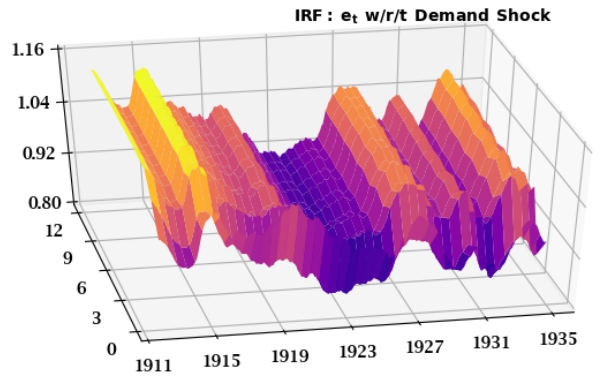

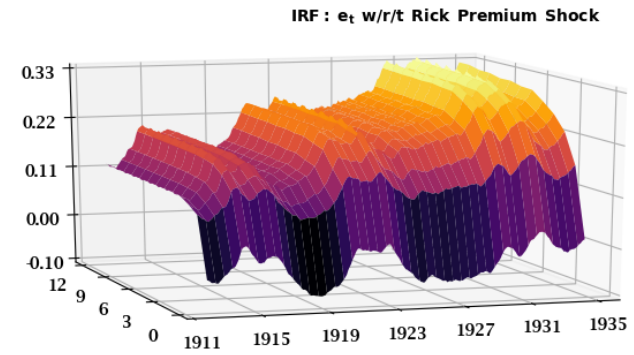

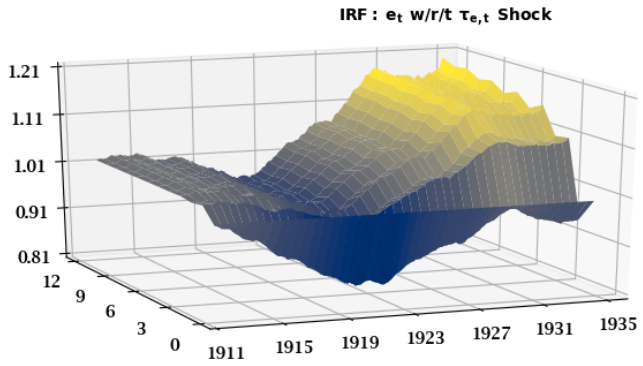

Notes: See the notes to figure A9.

Figure A13: Posterior Median FEVDs of i_t on the China-U.K. Sample, 1912M04 to 1934M09

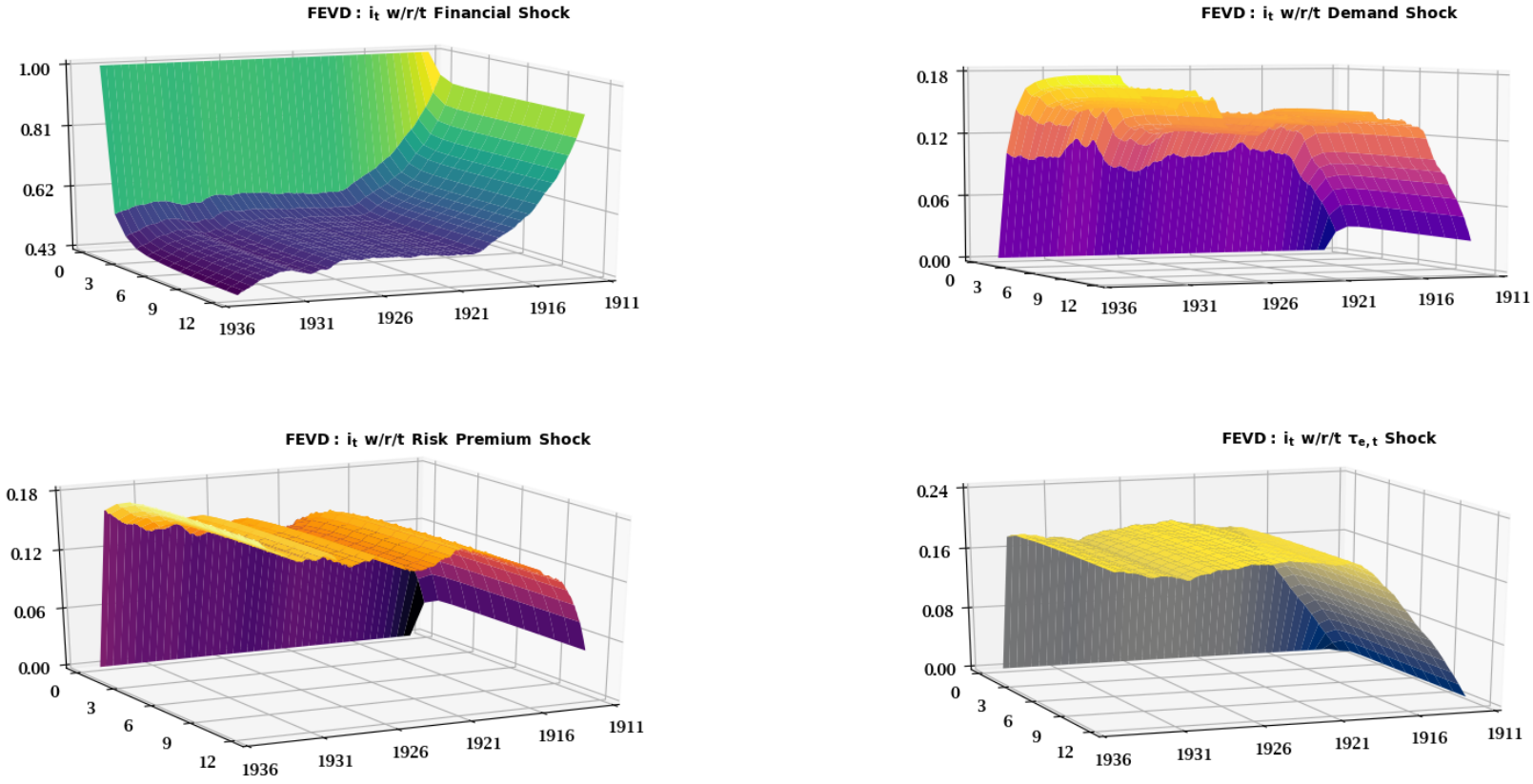

Notes: The median FEVDs are computed on the posterior distribution of TVP-SV-SVAR(2)-BL conditional on $y_{CUK,1:T}$ and our priors.

Figure A14: Posterior Median FEVDs of π_t on the China-U.K. Sample, 1912M04 to 1934M09

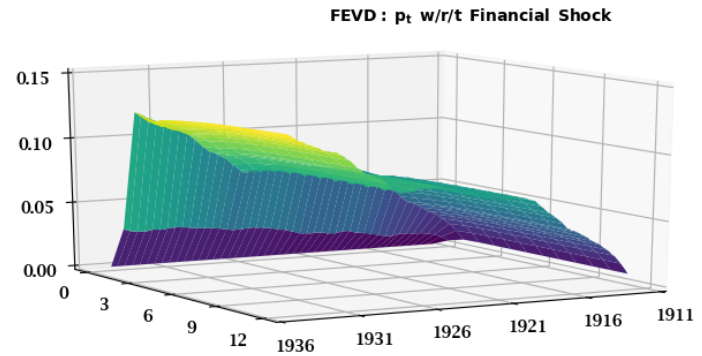

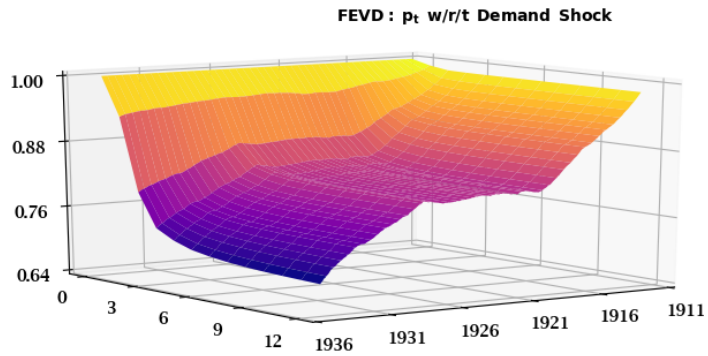

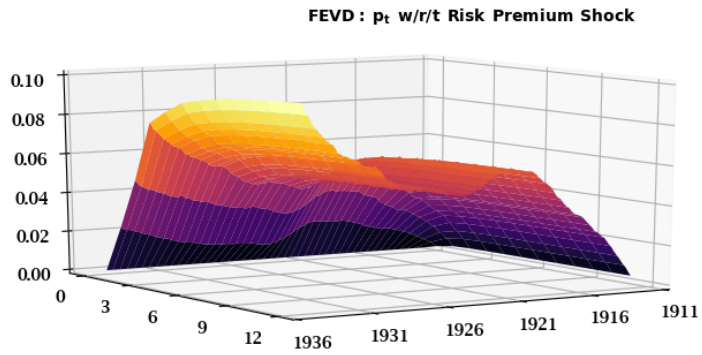

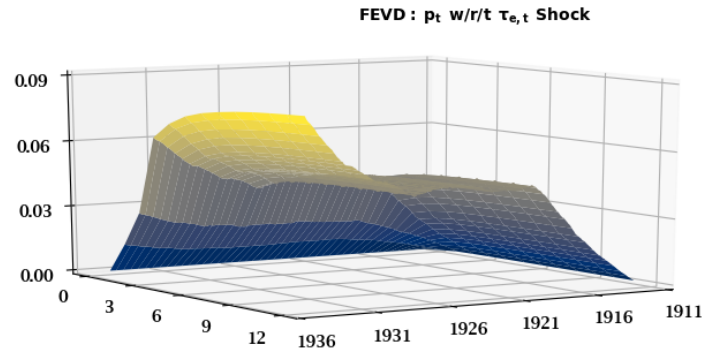

Notes: See the notes to figure A13.

Figure A15: Posterior Median FEVDs of ρ_t on the China-U.K. Sample, 1912M04 to 1934M09

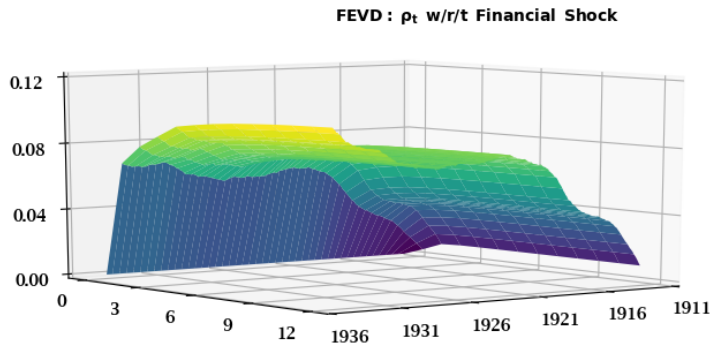

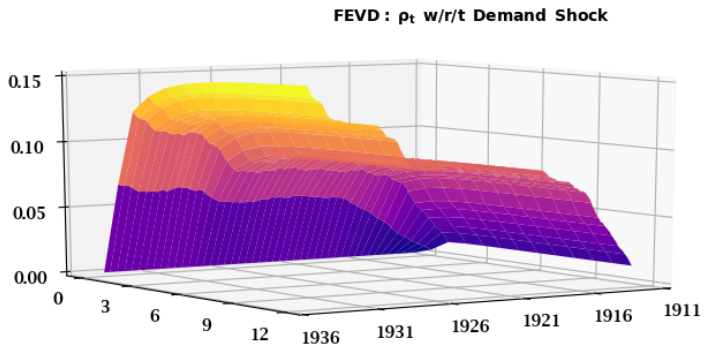

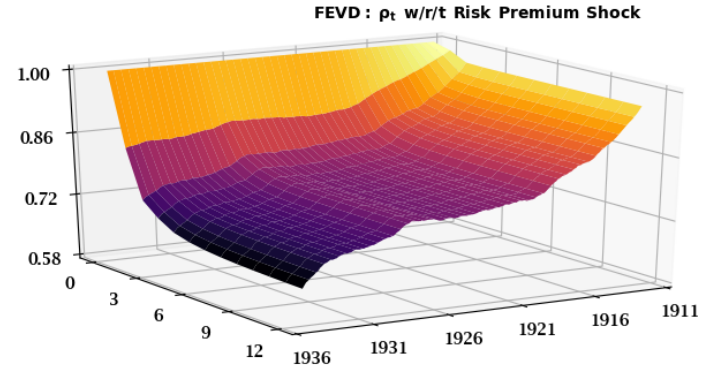

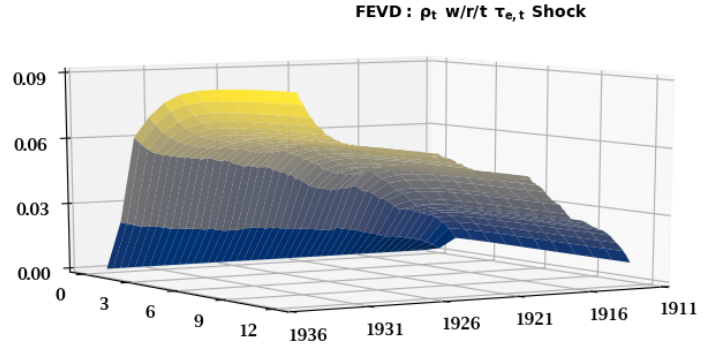

Notes: See the notes to figure A13.

Figure A16: Posterior Median FEVDs of Δe_t on the China-U.K. Sample, 1912M04 to 1934M09

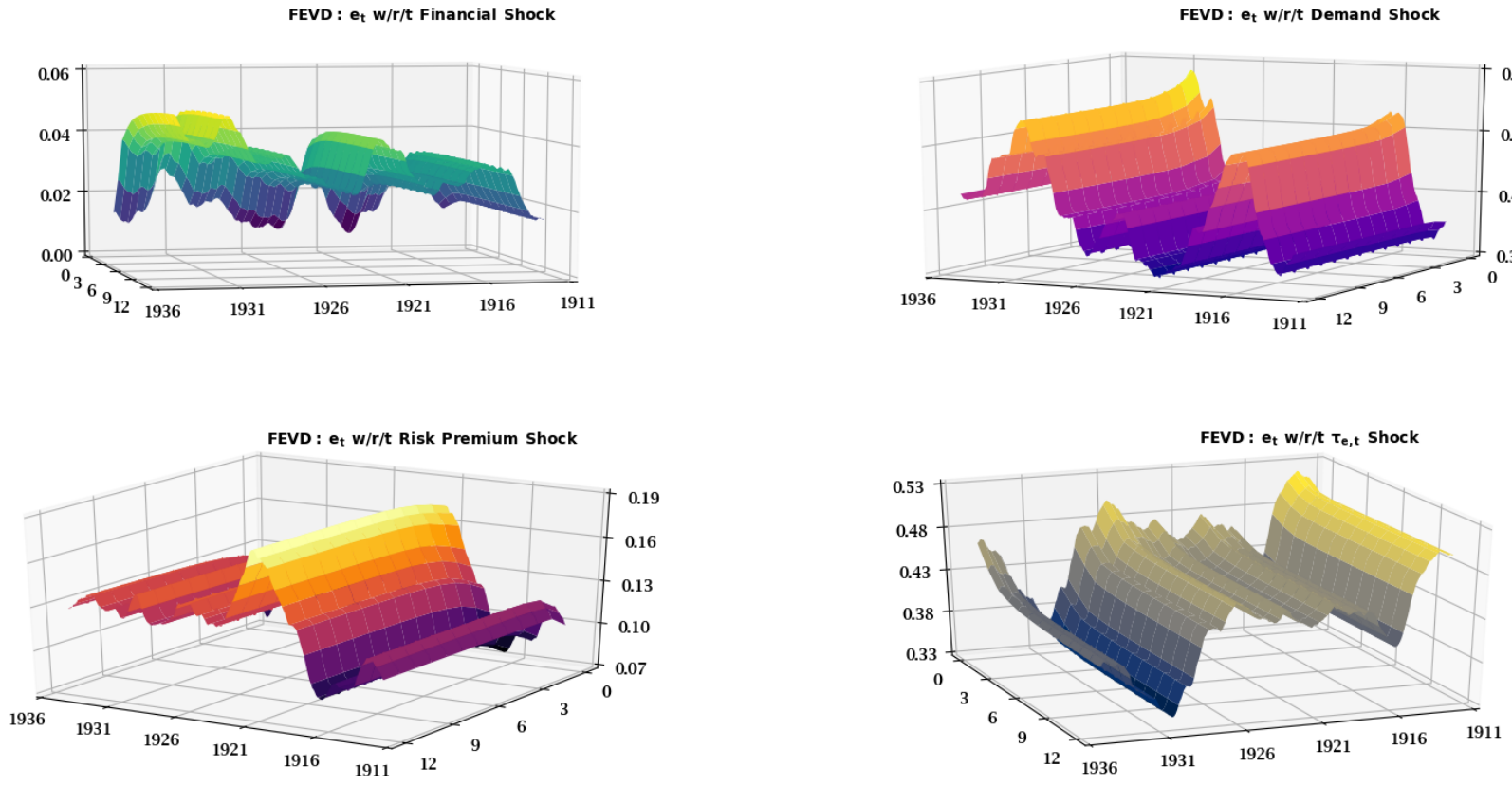

Notes: See the notes to figure A13.

Figure A17: Posterior Median FEVDs of i_t on the China-U.S. Sample, 1912M04 to 1934M09

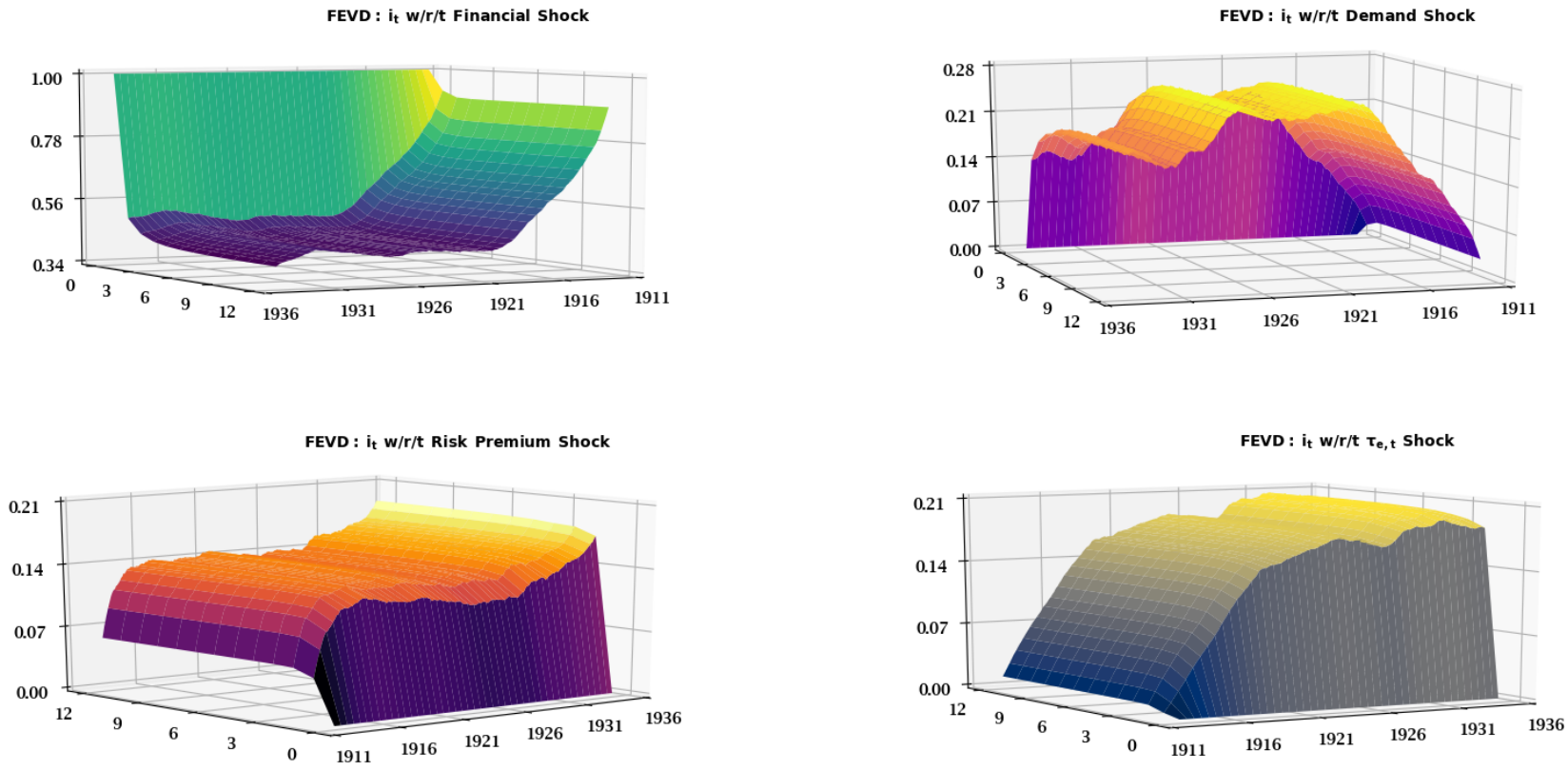

Notes: The median FEVDs are computed on the posterior distribution of TVP-SV-SVAR(2)-BL conditional on $y_{CUS,1:T}$ and our priors.

Figure A18: Posterior Median FEVDs of π_t on the China-U.S. Sample, 1912M04 to 1934M09

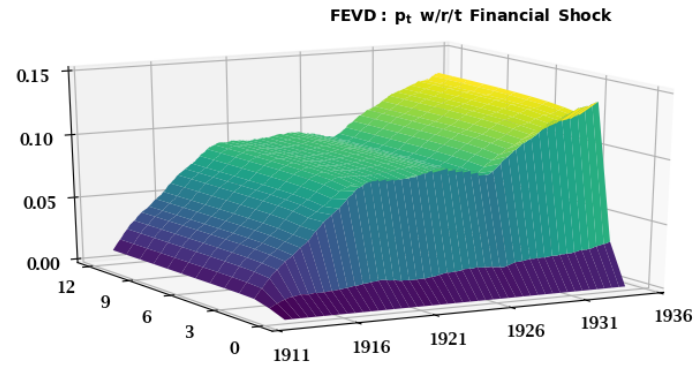

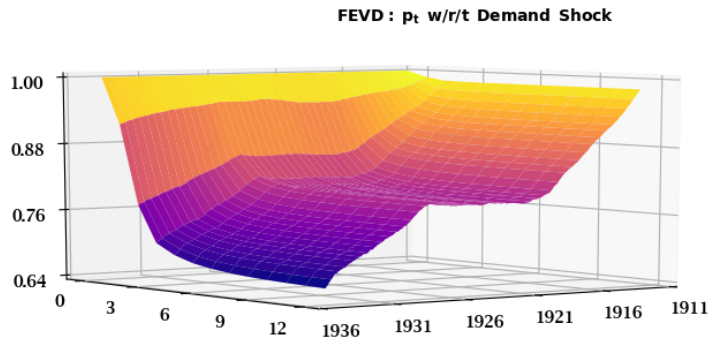

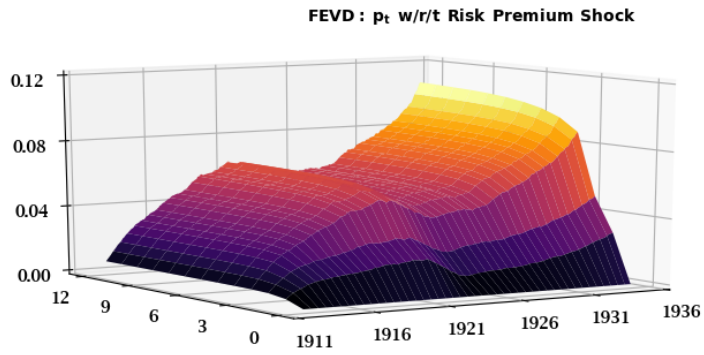

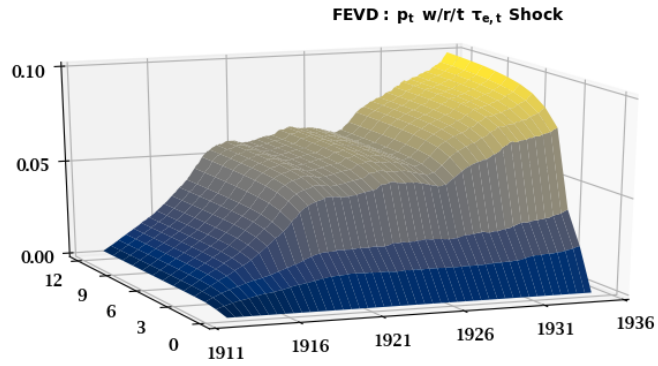

Notes: See the notes to figure A17.

Figure A19: Posterior Median FEVDs of ρ_t on the China-U.S. Sample, 1912M04 to 1934M09

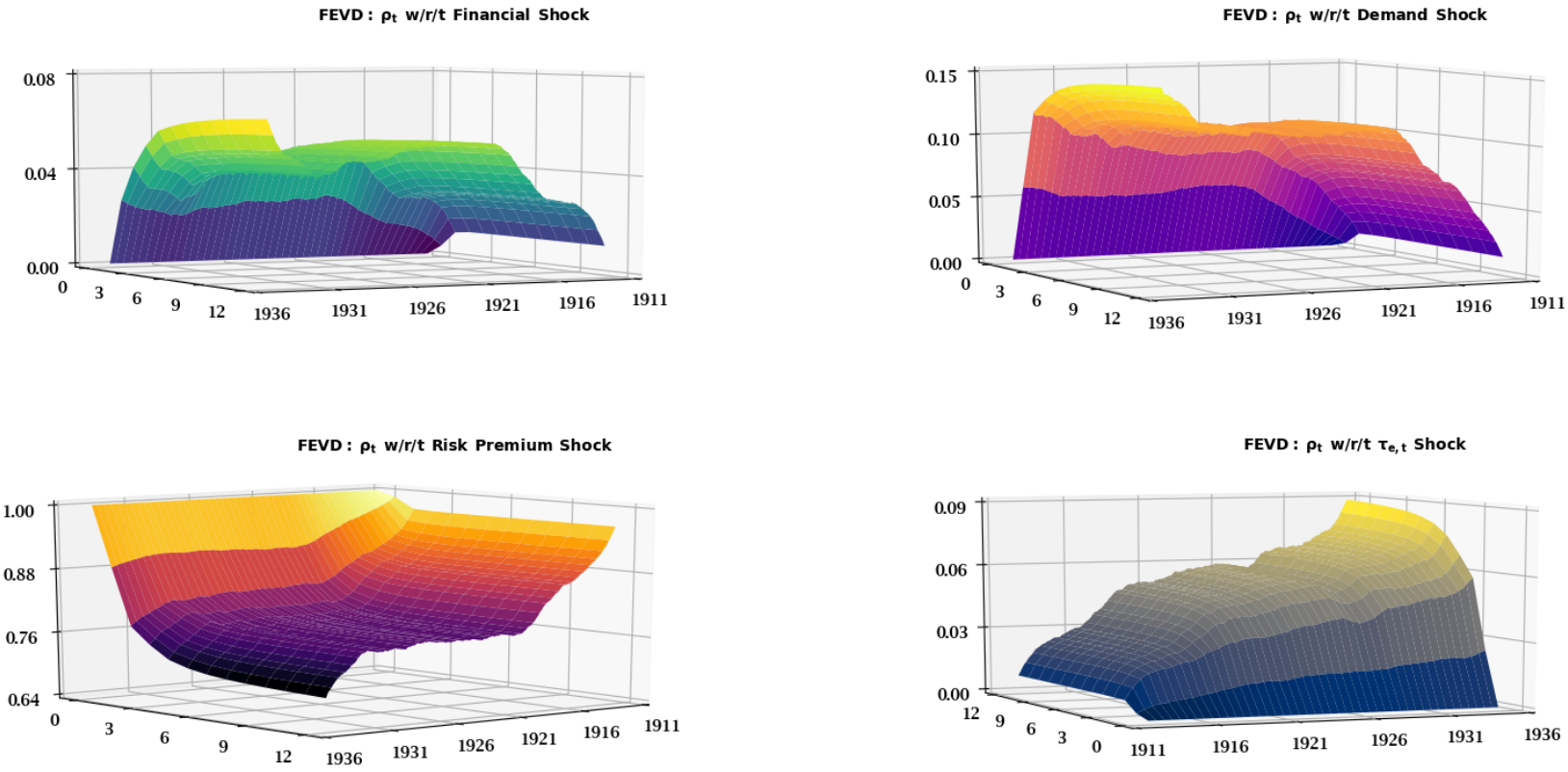

Notes: See the notes to figure A17.

Figure A20: Posterior Median FEVDs of Δe_t on the China-U.S. Sample, 1912M04 to 1934M09

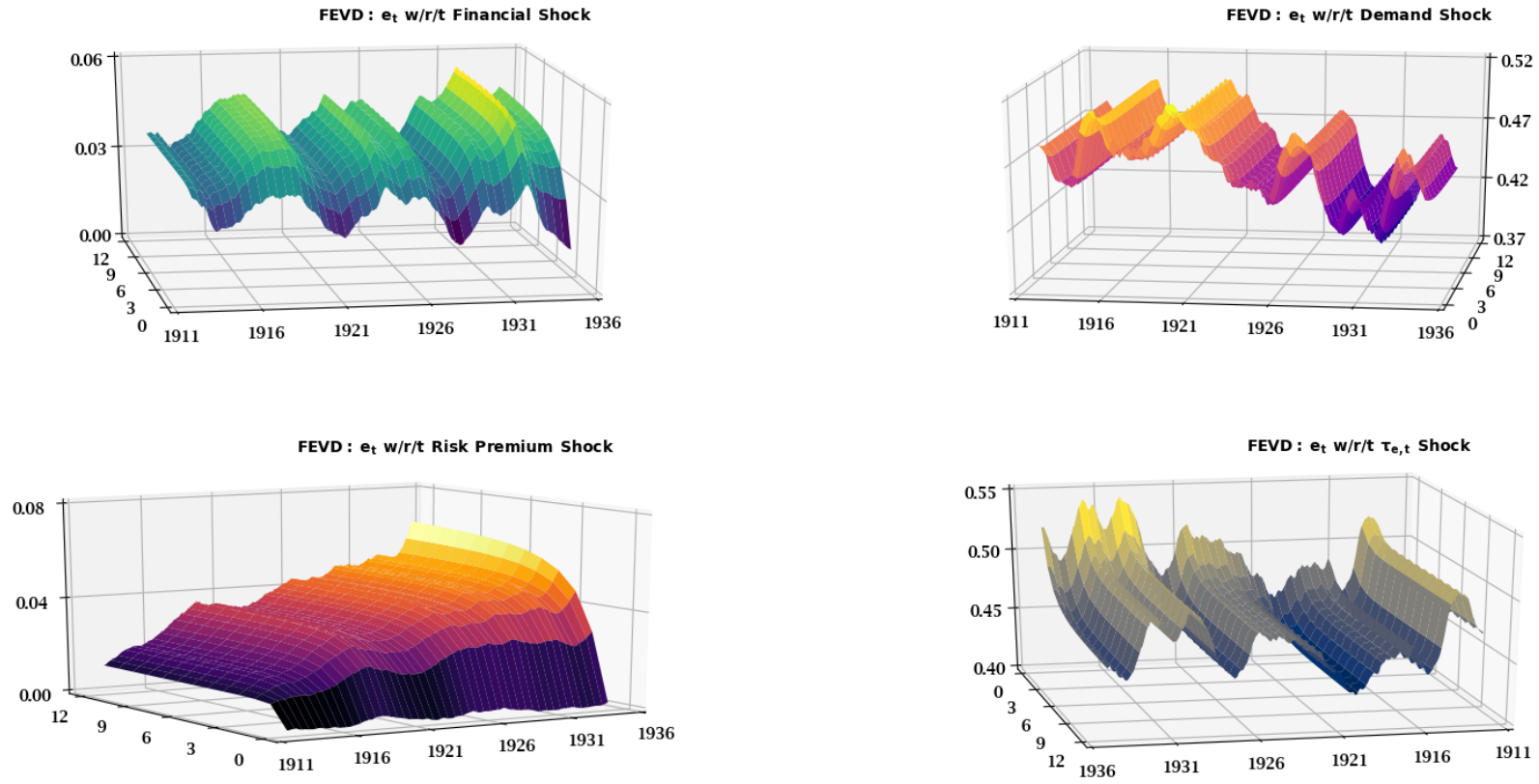

Notes: See the notes to figure A17.